

POLARIZING PROPERTIES OF PULVERIZED MATERIALS;  
APPLICATION TO THE LUNAR SURFACE

by

Samuel Frank Pellicori

---

A Thesis Submitted to the Faculty of the  
COMMITTEE ON OPTICAL SCIENCES

In Partial Fulfillment of the Requirements  
For the Degree of

MASTER OF SCIENCE

In the Graduate College

THE UNIVERSITY OF ARIZONA

1 9 6 9

STATEMENT BY AUTHOR

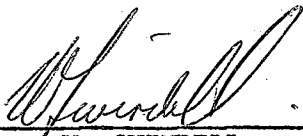
This thesis has been submitted in partial fulfillment of requirements for an advanced degree at The University of Arizona and is deposited in the University Library to be made available to borrowers under rules of the Library.

Brief quotations from this thesis are allowable without special permission, provided that accurate acknowledgment of source is made. Requests for permission for extended quotation from or reproduction of this manuscript in whole or in part may be granted by the head of the major department or the Dean of the Graduate College when in his judgment the proposed use of the material is in the interests of scholarship. In all other instances, however, permission must be obtained from the author.

SIGNED: Samuel Frank Pellicori

APPROVAL BY THESIS DIRECTOR

This thesis has been approved on the date shown below:



W. SWINDELL  
Professor of Optical Sciences

May 14 1969

Date

#### ACKNOWLEDGEMENTS

I am indebted to my advisors: Drs. W. Swindell, R. H. Noble, and T. Gehrels for suggestions and guidance in the preparation of this thesis. Dr. Gehrels, who provided support and laboratory space for several years, also provided me with an invaluable education in polarimetric techniques and analysis. His own lunar research raised many questions in my mind and, in part, provided some of the incentive for my research. Many people contributed to the development of the automatic polarimeter. Dr. G. V. Coyne collected some of the Hawaiian volcanic rocks, and allowed me to cooperate in a joint program with him on whole Moon polarimetry. The technical and secretarial staff of the Lunar and Planetary Laboratory offered their generous cooperation. Lastly, Ruth H. Pellicori assisted with some of the lunar observations, inked the drawings, and typed and proofread the first draft. The work was supported by the National Aeronautics and Space Administration.

## TABLE OF CONTENTS

	Page
LIST OF ILLUSTRATIONS.....	vi
LIST OF TABLES.....	viii
ABSTRACT.....	ix
I. INTRODUCTION.....	1
II. HISTORY OF LUNAR POLARIZATION MEASUREMENTS AND RELATED LABORATORY STUDIES.....	7
III. COLLECTION OF DATA ON THE INTEGRATED LIGHT FROM THE LUNAR DISK.....	21
Introduction.....	21
Development of an Automatic Polarimeter for Measurements of the Integrated Lunar Disk.....	21
Theory of Operation.....	22
Reduction Routine.....	27
Optics of the Instrument.....	28
Errors Inherent in the Design.....	33
Results.....	35
IV. COLLECTION OF DATA ON SELECTED LUNAR REGIONS.....	41
Introduction.....	41
Results.....	44
V. ANALYSIS OF THE NEW LUNAR DATA.....	50
The Polarization vs Brightness Relationship.....	50
VI. LABORATORY POLARIZATION STUDIES ON ROCK AND CHEMICAL POWDERS.....	53
Introduction.....	53
Apparatus.....	58
Lunar Context.....	61
Results.....	63
Opaque Materials.....	63

TABLE OF CONTENTS--Continued

	Page
General Conclusions on Opaque Samples.....	69
Translucent Materials.....	72
General Conclusions on Transparent Samples.....	76
Discussion.....	76
Polarizing Properties of Materials	
as a Function of Opacity.....	76
Dependence on Particle Size.....	81
Dependence on Surface Compaction.....	82
Dependence on Composition.....	82
Depolarizing Efficiency.....	84
 VII. APPLICATION TO THE INTERPRETATION OF LUNAR SURFACE DATA.....	 86
Introduction.....	86
The Wavelength Dependence of Polarization.....	86
Reproduction of the Lunar Phase Angle	
of Polarization Maximum.....	87
Identification of Lunar Materials	
Through Phase Angle of Maximum Polarization.....	90
Differences Between the Maria and Terrae.....	91
Hypothetical Explanation of the Dependence	
of Polarization on Phase Angle.....	96
Check of the Hypothesis With Respect	
to the Phase Angle Dependence of the Lunar Colors....	100
 VIII. CONCLUSIONS.....	 103
Summary.....	103
Recommendations for Future Research.....	105
 LIST OF REFERENCES.....	 107

## LIST OF ILLUSTRATIONS

Figure	Page
1a. Scattering geometry from a surface.....	5
1b. Illumination and phase angle geometry for the Moon.....	5
2. Analysis of electric vector into four components by two Wollaston prisms.....	23
3. Optical schematic of polarimeter.....	30
4. Polarization vs phase angle for the whole Moon at five wavelengths.....	36
5. Distribution of maria and terrae on the lunar disk.....	39
6. Location of examples of "pure" topography observed polarimetrically.....	43
7. Average polarization for the various topographical types.....	48
8. Average polarization values of the topographical types normalized at 0.54 $\mu\text{m}$ .....	51
9. Photomicrograph of lava powder No. 1, consisting of particles $\leq 37 \mu\text{m}$ size at phase angle of $0^\circ$ .....	59
10. Photomicrograph of lava powder No. 1 at phase angle $55^\circ$ .....	59
11. Schematic representation of laboratory apparatus.....	60
12. Polarization vs wavelength for solid surfaces.....	60
13. Polarization of black basalt powder of three sizes, sample No. 1.....	64
14. Polarization of Olivine basalt powder, sample No. 5.....	64
15. Olivine basalt, sample No. 5, at $0^\circ$ phase angle. Size 37-74 $\mu\text{m}$ washed.....	65
16. Olivine basalt, sample No. 5, at $180^\circ$ phase angle (transmission), size 37-74 $\mu\text{m}$ .....	65

Figure	Page
17. Polarization of frothy Pahoehoe lava, sample No. 7.....	66
18. Polarization of mixtures of carbon and sulfur.....	66
19. Sample No. 7, frothy Pahoehoe basalt at 0° phase angle, size $\leq 37 \mu\text{m}$ .....	67
20. Sample No. 7, 55° phase angle, sizes $\leq 37 \mu\text{m}$ .....	67
21. Polarizations of <u>aa</u> lavas, sizes $\leq 37 \mu\text{m}$ .....	70
22. Polarizations of iron compounds, all $\leq 37 \mu\text{m}$ .....	70
23. Photomicrograph of <u>aa</u> lava No. 8, 0° phase angle, size 37-74 $\mu\text{m}$ .....	71
24. <u>Aa</u> lava No. 8, 180° phase angle (transmission), size 37-74 $\mu\text{m}$ .....	71
25. Olivine, No. 15, size $\leq 37 \mu\text{m}$ pressed and not pressed, 37-74 $\mu\text{m}$ .....	73
26. Sulfur, size $\leq 37 \mu\text{m}$ , compacted and poured surfaces.....	73
27. Cobalt chloride polarization and transmission. Magnesium oxide (smoked) polarization.....	74
28. Olivine, 55° phase angle, 37-74 $\mu\text{m}$ size.....	75
29. Frothy Pahoehoe, No. 7, 180° phase angle (transmission), 37-74 $\mu\text{m}$ , washed of smaller particles.....	75
30. Depolarizing abilities of translucent and opaque powders as a function of wavelength.....	78
31. Black basalt, sample No. 1, 37-74 $\mu\text{m}$ washed of smaller particles, 180° phase angle (transmission).....	80
32. Reflectivity data of Adams and Filice (1967) replotted.....	92
33. Vertical cross section through microstructure of surface built from micro-meter size particles.....	98

## LIST OF TABLES

Tables	Page
I. Passband Characteristics.....	37
II. Polarizations of Lunar Regions.....	45
III. Effective Passband Characteristics for Laboratory Work.....	55
IV. Laboratory Polarimetry Samples.....	56
V. Lunar and Laboratory Values of $dP/d\lambda$ for $.33 \leq \lambda \leq .43 \mu$ , $\alpha \approx 90^\circ$ , and Two Size Distributions.....	88
VI. Percentage Polarization of Regions at Small Phase Angles.....	101



## ABSTRACT

Photoelectric measurements of the degree of linear polarization of integrated Moonlight and of specific lunar topographical regions over the range of wavelengths 3200 to 5500 Å are reported. The design of an automatic polarimeter for the integrated Moonlight measurements is described.

Investigations are made of pulverized volcanic lavas and of pure chemicals. The influence of particle size distribution, state of surface compaction, composition, wavelength, and phase angle on polarizing characteristics of pulverized materials are studied with the aim of contributing to the determinations of lunar and planetary surfaces.

It is found that the wavelength dependence of the polarization of the Moon, (and of Mercury and Mars) can be explained by the increase in the mean internal optical path length in their particles with decreasing wavelength. This causes the proportion of the light scattered by the particle surfaces (giving high polarization) to the light scattered by the interiors (having low polarization) to increase with decreasing wavelength. The lunar surface appears to consist of 30 to 60  $\mu\text{m}$  sized particles which are translucent, not opaque. Pulverized basalt is a suitable material.

Polarimetry provides information about the optical properties of remote surfaces that can be used to help deduce, by empirical comparison, particle size distributions, surface textures, and compositions.

Remote detection of the presence of a specific material whose polarizing properties are known is possible. However, unambiguous identification of a mineral species by polarimetry alone is doubtful. Contrary to the suggestion by other investigators, Brewster's law (Fresnel's reflection laws) is not applicable to the unambiguous determination of the effective refractive index of a diffusely scattering surface.

## SECTION I

### INTRODUCTION

Sagredo. "Will the new observations and discoveries made with this admirable instrument never cease?"

Salviati. "If its progress follows the course of other great inventions, one may hope that in time things will be seen which we cannot even imagine at present."

-- Galileo, Dialogue Concerning the Two Chief World Systems, 1632

Measurements of the total intensity of light as a function of wavelength by means of filter photometry or spectroscopy provide information about the spectral reflecting and absorbing properties of a diffusely scattering surface. Photography reveals the large-scale structural features. The spectral brightness of a diffusely reflecting surface is dependent on the composition of the surface, and relatively insensitive to scattering angle and surface microstructure. Analysis by polarimetric techniques of the noncoherent electric-vector components scattered by a surface into

various azimuths provides information about the scattering efficiencies in these azimuths. It is known that these scattering efficiencies are strongly dependent upon the wavelength, the surface microtexture, the material composition, and the angle between the observer, the scatterer and the light source ("phase angle"). Thus, polarimetry provides more information about the nature of remote surfaces than intensity and imaging measurements do.

Analysis of light into measurable quantities that constitute the Stokes parameters for linear polarization and quasi-monochromatic light allows comparison between the surfaces of the Moon, Mercury, Mars and the asteroids and laboratory samples.

This thesis is concerned with the character of polarization, by scattering from powdered surfaces as a function of wavelength, of scattering angle, and of composition. Inferences are drawn toward the comparisons with the optical properties of the lunar surface.

Although it has been known since 1811 (Sec. II) that the light from the Moon is polarized, a universally accepted, detailed explanation of the polarizing mechanism has not been developed. A theory that explains the observed polarimetric behavior must accommodate the photometric behavior, and conversely. An illustration of the peculiar scattering nature of the lunar surface is given by the observation that a sphere with a diffusing surface (smoked magnesium oxide) which is illuminated from behind the observer (i.e., near zero phase angle) has a central area that is brighter than the limb. The full Moon, however, exhibits no measurable limb darkening.

The optical properties of the lunar surface depend on its chemical composition, particle size, state of compaction, microstructure, wavelength and phase angle. Because some of these parameters are influenced to an unknown degree by solar electromagnetic and particulate irradiation, by meteoritic influx, and by volcanic activity, analytic theories explaining the optical scattering properties are difficult to formulate. Although either the photometric or the polarimetric function can be reproduced with powders in the laboratory, a surface which, in detail, satisfies both has not been found.

The present work consists of five major parts: a brief summary of the history of lunar polarization measurements and associated laboratory comparisons (Sec. II), the collection of more definitive data on the integrated lunar disk (Sec. III) and on lunar regions (Sec. IV), investigations of the scattering properties of various materials (Sec. V), discussions of the data in the light of the laboratory results (Sec. V), and some inferences about lunar surface composition, particle sizes, and possible polarizing mechanisms (Sec. VI).

The collection of new data on the integrated disk required a new polarimeter. Its design and development is described in Section III. Data was taken over all accessible phase angles and wavelengths between  $.33$  and  $.56 \mu$ . The data on the regions was taken over the above span of wavelengths, but was restricted to phase angle near the maximum of polarization to facilitate intercomparison of the topographic types. The polarizing properties of powdered opaque and translucent materials were studied over the wavelength range  $.32$  to  $.70 \mu$ ,

and at phase angles  $\alpha \geq 90^\circ$ . Compositions were varied to study the effect of refractive index on P and the angle of maximum P, particle sizes were  $74 \mu\text{m}$  and  $37 \mu\text{m}$  for the majority of experiments. The primary purpose was to define more clearly the roles of opacity, refractive index, and to a lesser extent particle size on the wavelength dependence of the polarization and  $\alpha_M$ . A secondary goal was to apply some of the findings on materials to the lunar data and thereby arrive at some conclusions concerning the nature of the lunar surface.

The quantities to be discussed are defined as follows. Fig. 1a shows a scattering surface illuminated by a source to the right and observed from the left. The plane of scattering is the plane which contains the source, the scatterer, and the receiver. The angle subtended at the scatterer by the directions to the source and the receiver is the phase angle,  $\alpha$  (Fig. 1b). In general, the normal to the surface,  $\underline{N}$ , is not in the plane of scattering, but is out of this plane by the angle  $\underline{1}$ . However, for all of our considerations (the lunar surface and powders) the brightness and polarization are independent of  $\underline{1}$ , as evidenced by the independence of lunar region brightness on latitude and by the work of Dollfus (1962) and Coffeen (1965). The angles of incidence and emergence,  $\underline{i}$  and  $\underline{e}$ , for the Moon lie within  $\pm 5^\circ$  of being in the plane of scattering. Thus,  $\alpha = i + e$ . For the Moon,  $\alpha = -90^\circ$  at first quarter illumination, and  $\alpha = +90^\circ$  at last quarter.  $\alpha = 0^\circ$  at full Moon. The phase angle at which maximum polarization occurs is  $\alpha_M$ . Reflectance,  $R(\lambda)$ , is the ratio of light flux scattered by a diffuse surface in all directions to the collimated

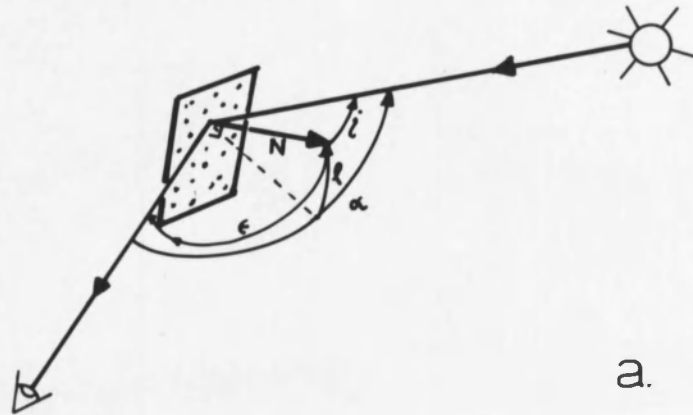


Fig. 1a. Scattering geometry from a surface.

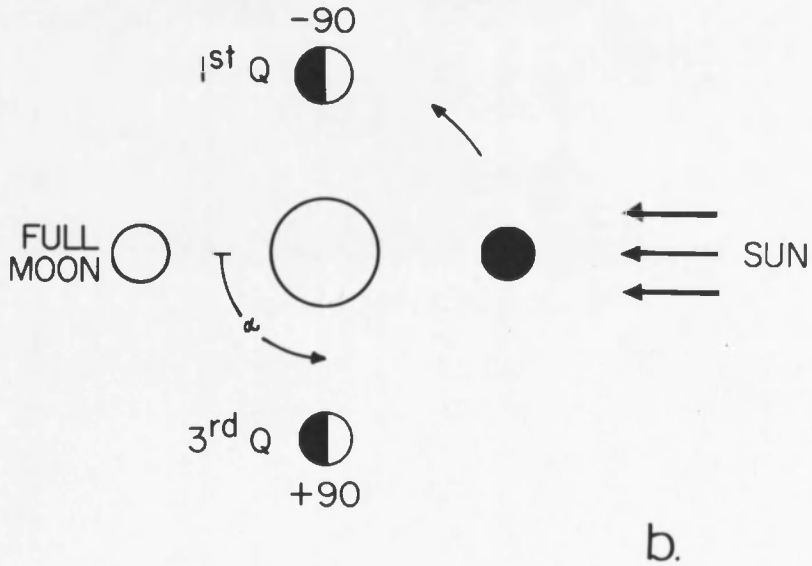


Fig. 1b. Illumination and phase angle geometry for the Moon.

incident flux, and is often called normal albedo.

The percentage polarization,  $\underline{P}$ , is defined as

$$\underline{P}(\lambda) = \frac{\underline{I}_M - \underline{I}_m}{\underline{I}_M + \underline{I}_m} \cdot 100$$

where  $\underline{I}_M$  is the maximum component of the electric vector, and  $\underline{I}_m$  is the minimum. When  $\underline{I}_M$  lies in a plane perpendicular to the plane of scattering,  $\underline{P}$  is called positive, when it lies in the plane of scattering it is negative. The position angle  $\theta$  of the electric vector maximum is measured with respect to the perpendicular to the plane of scattering;  $\theta = 180^\circ$  for positive polarization,  $\theta = 90^\circ$  for negative. From observations mentioned in the Historical Summary (Sec. II) it appears that the elliptical polarization of Moonlight and of light scattered by powdered and solid laboratory samples is negligible, therefore, only linear polarization is considered in this work.



## SECTION II

### HISTORY OF LUNAR POLARIZATION MEASUREMENTS AND RELATED LABORATORY STUDIES

The history of the study of the polarizing properties of materials parallels, to a large degree, the history of the study of the light scattered by the Moon. Therefore, these histories will be discussed simultaneously.

Galileo's first telescopic observations of the Moon revealed to him that the darker areas are plains and the brighter areas are mountains (1632). He deduced from the observation that the lunar surface is uniformly bright, that the surface must be rough and diffusing rather than polished like a mirror. He also argued that the lunar surface is quite different from the terrestrial surface, is lifeless, and has no water. In those brief few hours after the birth of telescopic astronomy, Galileo had also correctly explained the shape of the Moon, the phases, the earthshine, eclipses, the reason why only one face of the Moon is seen, and had observed the effects of libration.

Huygens discovered that light is polarized when passed through a calcite crystal. Shortly after the discovery of polarization by reflection by Malus in 1808, Arago (1811) discovered that the light from the

Moon is polarized. Arago attributed this polarization to a lunar atmosphere. Provostaye and Desain (1852) studied, for the first time, the polarization of light scattered by solids. They discovered that the polarization is greatest for rays scattered at large angles from the surface normal and decreases as the angle to the normal is reduced. They found that dark or colored substances polarize more strongly than white ones, and that white substances such as white lead depolarize incident polarized light. For colored materials, the light which is polarized perpendicular to the plane of reflection is attenuated more than light polarized parallel to the plane of reflection. Verdet (1860) offered the theory that polarized light which is scattered internally by a particle is scattered randomly and thus depolarized. Sir David Brewster (1861) was one of the first to study polarization from rough and white surfaces, e.g., cloth, painted and unpainted wood, snow, ground glass, paper, etc. He was interested in discovering the cause of the partial polarization and the neutral points of the atmosphere. He recognized that the laws of polarization by polished surfaces are not applicable to rough or translucent bodies.

Secchi (1859) theorized that it was the lunar ground and not an atmosphere that caused Moonlight to be polarized. He found that the light from the maria (dark plains) has greater polarization than that from the terrae, and that the plane of polarization is perpendicular to the plane of scattering. Parsons (Third Earl of Rosse) observed Mare Crisium at several phases (1878) and confirmed Arago's earlier results that the polarization reaches a maximum (12%) at quadrature and

becomes zero at full Moon. He suggested that polarization measurements could be used to determine the refractive index of the lunar materials, but made no laboratory comparisons. Landerer (1890) studied ice and some igneous rocks having plane, polished surfaces in order to determine the angle of maximum polarization, and decided that vitrophyre did duplicate the maximum lunar angle. (Vitrophyre is a black rock consisting of sanidine, magnetite, and hornblende or some similar acidic mineral.)

Umov (1905) extended the work of Provostaye and Desain and found that polarized light of a given color will be depolarized by a substance that scatters that color efficiently, and that opaque substances return the incident polarization without alteration. He hypothesized that those wavelengths which are responsible for the color of a substance are those which are best able to penetrate it, and they are consequently depolarized by random internal scattering. The polarization is strongest for those wavelengths most strongly absorbed. This property has become known as the "Umov Effect", which has been offered as a mechanism that "explains" the lunar polarization versus wavelength characteristics.

Salet (1922) found that the angle of maximum polarization of a rock varies with the degree of polish, and thus Landerer's result with polished vitrophyre became questionable. Galileo had long before reasoned that the lunar surface must be rough because of its scattering properties.

Woronkoff and Pokrowski (1924) studied the polarization caused by reflection from diffuse surfaces having different absorptions as a function of angles of reflection and incidence. They reasoned that if the absorption is high, the light is scattered entirely from the surface and, therefore, Brewster's law can be used to determine the refractive index. Note that this contradicts the statement by Brewster himself that the laws of reflection by polished surfaces do not apply to rough surfaces. Woronkoff and Pokrowski found that as the absorption decreases, the angle of the maximum value of polarization shifts toward larger angles of reflection. However, when a material is pulverized the determined value of refractive index is smaller than for the solid bulk material. They also found that light coming from the interior can be considered as unpolarized, and contributes more to the total light returned at small incidence angles. This decreases the polarization at small phase angles.

Barabashev (1926) studied carborundum and glass grains and found that the polarization is smaller for smaller grain size. By comparing the polarization and reflectivity of lunar maria and terrae with laboratory samples, he found that a yellowish sand corresponded best to the terrae, and a lava corresponded to the maria.

F. E. Wright, chairman of the Carnegie Institution's Moon Committee, reported on a project of lunar and laboratory studies (1927-1938). Although the Committee's researches contributed much knowledge on the natures and causes of polarization on various materials, their conclusions concerning the Moon, which have been highly

respected by many researchers in the field, have been contradicted. They concluded (1927a&b) from studies of basalts, meteorites, and glasses, that dark colored rocks high in silica and low in iron must exist on the Moon because the light reflected by quartz porphyries, pumices and granites approach the lunar values. Basalts, peridotites, serpentines, gabbros (basic or ultra basic compositions), etc., do not exist on the Moon according to their optical findings. They studied negative polarization (1935) and found a large range of phase angles where the polarization changes from negative to positive for terrestrial materials. They found that some substances do not give negative polarization. For rough materials the polarization is attributed to diffraction and multiple scattering, and only negligibly to specular reflection (1936). They concluded, in connection with studies on diffraction gratings, that negative polarization is caused by diffraction rather than reflection. They confirmed that dark materials polarize more strongly than bright ones because in the latter case light which has penetrated can be multiply scattered and returned with a different polarization azimuth (1937). The causes of polarization, according to the Moon Committee, are diffraction combined with absorption and internal and external reflection, and not solely reflection and refraction. They concluded that the study of negative polarization is of little value as a diagnostic tool. Their conclusion (1938) was that the lunar materials are light and porous, and their polarizing properties can be reproduced by pumice and volcanic ashes which are high in silica (acidic). Wright's studies of lunar regions revealed

no dependence of the polarization on wavelength. This is attributed to his low accuracy which was  $\pm 1\%$  to  $\pm 10\%$ .

Lyot (1929) had concluded earlier that ground up volcanic ashes do reproduce the lunar polarization. In 1922 Lyot began his study of the polarization of lunar regions and of the integrated disk as a function of phase angle, which was to become the classical reference for lunar data up to the mid-Sixties (1929). He also studied clay, ores, lavas and volcanic ashes for comparison with the lunar data. His principal lunar observations are briefly reviewed here. Lyot's curve is replotted as the dashed line in Fig. 4, p. 36. The plane of vibration of the electric vector is the same at every point on the Moon; it is perpendicular to the plane of scattering for phase angles greater than  $|24^\circ|$  and in the plane for angles 0 to  $|24^\circ|$ . At  $\pm 24^\circ$  and at  $0^\circ$  (full Moon) the polarization goes to zero. For the integrated light the maximum reaches  $+8.8\%$  at  $\alpha = -94^\circ$  (near first quarter) because there are more maria illuminated during last quarter. The minimum of  $-1.2\%$  is reached at  $\pm 11^\circ$  phase angle. There is no detectable difference in polarization between comparable regions near the center and near the edge of the disk. Dependence is found on the angle of incidence but only near the terminator where the angle is large. Lyot made the first search for elliptical polarization on the Moon and concluded that it must be less than  $0.3\%$ .

Lyot studied powdered compounds (chlorides and nitrates) of different refractive indices, and found that the maximum degree and angle of polarization are independent of index. Grain shape seemed to

have a greater influence than index. He verified the conclusion of Woronkoff and Pokrowski that light which returns from the interior of a substance is polarized less, and that the maximum polarization occurs at greater phase angle. However, the light reflected from the surface gives negative polarization. For lavas, the porous ones have low polarization with the maximum displaced toward small phase angle. Strongly vitrified lavas have large polarization and weak or non-existent negative values. The best match to the lunar data was given by ashes of the Vesuvius Volcano. He theorized that the negative branch is caused by diffraction. The observation that for some substances the negative branch is caused by the surface, and for others by the interior puzzled Lyot. He confirmed Secchi's result of the inverse relationship between degree of polarization and brightness on the Moon.

The first photoelectric observations of polarization were done by Ohman (1945), and confirmed Lyot's results.

Through the 1950's Dollfus continued the studies of Lyot and Wright. His results are briefly reviewed now. His studies of vitreous surfaces showed that the polarization depends on the angle of inclination of the surface normal from the illumination and observation directions (1962). He concludes that vitreous surfaces do not exist on the Moon because either a bright reflection or high polarization would be detected. Studies of transparent grains showed that quartz and chalky sediments do not satisfy the lunar values. With opaque and transparent rough scatterers the degree of polarization was

found not to depend on the inclination of the surface. The same holds for powdered opaque materials, but the negative branch is more pronounced than with partly absorbing surfaces. He attributed negative polarization to multiple diffraction and diffusion of light between the grains. It increases with decreasing particle size, and Dollfus concludes that it reaches a maximum with perfectly opaque substances which are pulverized. He therefore concludes that the lunar surface must be covered with a very absorbing powder similar to volcanic ash, and has a porous structure. He proposed that the polarization was determined by Fresnel's reflection laws applied to rays scattered by the surface and by the interior of materials. Dollfus (1955) observed that the ashen light from the Moon is more polarized in the blue light than in red.

Ohman (1945) suggested the use of detectors with different spectral responses to observe the lunar polarization. Gehrels (1959) found with a photoelectric polarimeter that the degree of polarization of lunar regions increases with decreasing wavelength. Teyfel (1959) also found this result with polarized spectrograms and explained it by the Umov effect. Sytinskaya (1956) related Lyot's polarization values to visible albedo  $R$  at full Moon by the following relation

$$P = .276 - 1.95 R, \quad .05 < R < .115.$$

By comparison between the colors of terrestrial rocks and lunar colors, Barabashev and Chekirda (1956) concluded that volcanic effusive rocks and their tuffs provided a close match to the lunar values.



"Ohman offered an explanation of negative polarization in terms of multiple reflection by cleavage surfaces forming a  $90^\circ$  angle (1955).

Ivanov and Toporetz (1956) developed a method for measuring the external and internal components of diffuse reflection using incident polarized light at azimuths parallel and perpendicular to the plane of scattering.

Kohan (1962) found, at variance with Lyot, the position angle of the plane of polarization of the Moon to rotate smoothly with respect to the plane of scattering as the phase angle is changed in the region  $0^\circ$  to  $\pm 40^\circ$ . Lyot found a sudden discontinuous shift between  $90^\circ$  and  $180^\circ$  at  $\alpha = \pm 24^\circ$ . Kohan also found this phenomenon for terrestrial rocks. The precision polarimetry of Gehrels, Coffeen and Owings (1964) agreed with the results of Lyot to an accuracy of  $\pm 3^\circ$ . Clarke (1964), on the other hand, agreed with Kohan, and also found the effect for Mars. Gehrels, et al (1964) has shown that the plane of polarization can undergo an apparent rotation if the conversion of the instrumental reference plane -- normally the plane of the ecliptic -- to the plane of scattering is not carefully done. Precision results on integrated Moonlight (Coyne and Pellicori, 1969) show that for phase angles greater than  $|20^\circ|$ , the plane is perpendicular to the ecliptic as Lyot and Gehrels found, but the existence of a systematic rotation of the electric vector toward an angle of  $0^\circ$  to the plane of scattering can not be ruled out for  $-20^\circ < \alpha < +20^\circ$ . The large scatter of the measurements for such small values of  $P$  makes them uncertain

since the position angle is directly proportional to the magnitude of P. The data of Gehrels on regions shows scatter as large as that obtained by Coyne and Pellicori i.e., as large as  $\pm 30^\circ$ .

Kohan worked on laboratory comparisons, and reported that the position angle does not depend on the degree of pulverization, or the angle of reflection. The same dependence of polarization on brightness was found for rocks as was found for the Moon. He found that for grain sizes less than 0.25 mm or greater than 1.0 mm the polarization curves do not differ much from each other and concluded that the degree of polarization can not be used to determine the scale of lunar particles. His best fits give ocherous limonite as simulating the maria, and volcanic tuff for the terrae, but the trends of the rotation of the plane of polarization are not analogous.

Interest in reproducing the lunar surface properties in the laboratory with the hope of being able to extrapolate to lunar surface composition and structure was stimulated by the United States' manned lunar landing programs. In the early 1960's several NASA funded industries began laboratory simulation studies. In general, photometric and colorimetric studies were initiated first.

Hapke and Van Horn (1963) offered a complicated theoretical photometric function which reproduced the lunar photometric behavior fairly closely, especially in Hapke's revised form (1966). The model is based on combinations of the Schönberg, Lommel-Seeliger, and Lambert scattering laws plus factors to provide back-scatter at large phase angles. The physical model is a low density layer of particles

randomly placed but having a structure ("fairy castle") composed of interstices that are interconnected. The shadowing that this complex structure produces at large phase angles diminishes as  $0^\circ$  phase angle is approached, and all the light which penetrated the structure is able to escape in the direction from which it came. Hapke and his co-workers did not attempt to reproduce the polarimetry until later, but they did contribute much of the early data on the suggested darkening of lunar grains by solar wind bombardment (1962).

Wehner, Rosenberg and KenKnight (1964) began polarimetric studies of basalts, obsidian, tuff, rhyolite, serpentine and granodiorite powders both irradiated with protons and helium ions and unirradiated. They found that the albedo, and correspondingly, the polarization to be dependent on the amount of irradiation. Longer irradiation decreased the albedo and increased the degree of polarization. They supported Hapke's earlier result that irradiation reduced metal oxides to metal and that a real chemical change is responsible for the darkening. Recently, there has been some question raised by Nash (1967) and Greer and Hapke (1967) about the possibility of vacuum oil decomposition and sputtering by accelerating electrodes being responsible for the darkening. Also, the Surveyor landers turned over lunar soil and revealed that the outer layer is lighter than the underlying particles.

Coffeen (1965) investigated some particles of volcanic ash  $< 37 \mu\text{m}$  diameter at wavelengths .36, .44 and .90  $\mu$ . No dependence of polarization was found on the orientation of his sifted ("fairy

castle") samples. His differential photometry of the powders showed a reddening with increased phase angle as Gehrels, et al. (1964) discovered for the Moon.

Egan and Smith (1965) began a program of measurements on natural surfaces and simulated lunar surfaces including volcanic ashes, coral, silver chloride, etc. They varied the sample orientation to simulate various lunar latitudes and longitudes. Most of the samples were independent of these parameters just as the lunar surface is. They later varied particle size, wavelength, albedo and porosity (Egan, Smith, McCoyd, 1966). They were able to simulate the polarimetric properties of maria with particles of volcanic ash from Haleakala, Hawaii having sizes 37 to 88  $\mu\text{m}$ , and with furnace slag smaller than 37  $\mu\text{m}$ . Craters were simulated by ash smaller than 37  $\mu\text{m}$  and by furnace slag smaller than 1  $\mu\text{m}$  size. The samples were not irradiated. An important point attributed to Hapke is that although volcanic ashes reproduce the lunar polarimetric function, they do not reproduce the photometric function.

The successful landings of Luna 9 and Surveyors I, III, V, VI, and VII confirmed with close-up photography the conclusion deduced by remote optical measurements as long ago as Galileo's 1632 observations that the lunar surface is indeed powdered and complex. The modern day optical (polarimetric and photometric) inferences, that the particle sizes must be less than 1 mm and the microstructure very intricate, were confirmed by photographs taken at various phase angles (illumination angles) of the footpad impressions of the Surveyors.

The change in photometric behavior when the lunar soil is compacted indicates that the complex, underdense structure has been crushed. The limiting resolution of the photographs is 1 mm, yet none of the particles in the soil or sprayed onto the solar panels is even nearly resolved. The conclusions based on the adhesion of fine light scattering dust on the viewing mirrors and on the change in the intricate shadow casting structure of the footpad impressions is that the lunar particles must be nearly 10  $\mu\text{m}$  size (Gault, Collins, Gold, Green, Kuiper, Masursky, O'Keefe, Phinney and Shoemaker, 1967).

Chemical analyses by Surveyors V, VI, and VII report a basaltic composition, resembling terrestrial basalts, rather than an acidic or meteoritic composition.

It is fallacious to conclude that further laboratory and telescope research is of decreased value now that man is about to sample an actual piece of the lunar surface. In the first place, the Surveyors photographed only very localized regions which incidently, except for Surveyor VII, were samples of rather featureless manned landing terrain. Chemical analyses were limited to distances only one meter from the space craft. The first Apollo flights will similarly sample areas only within a few hundred yards of the landing. More importantly, however, the results from the lunar programs serve to provide invaluable calibration of our remote sensing techniques and conclusions, and thus establish confidence in our applications of them to the studies of other planets and their satellites.

It therefore seems appropriate to systematize at this time (before the lunar landing) our methods of interpreting surface studies with the aid of remote polarimetry.

### SECTION III

#### COLLECTION OF DATA ON THE INTEGRATED LIGHT FROM THE LUNAR DISK

##### Introduction

Lyot (1929) was the first to study the polarization vs phase angle properties of the integrated disk of the Moon. His results have become the classical reference on lunar polarization information. The polarimeter he designed used a birefringent Savart plate to produce visually observed fringes when polarization is present in the incident light; a thin, tiltable sheet of celluloid to polarize the beam and thereby cancel the incident polarization, and a rotatable polarizer to make the fringes visible. Knowledge of the polarization introduced by the tiltable plate from Fresnel's laws allowed determination of the polarization. Lyot's main results were summarized in Sec. II.

The dependence of P on wavelength for lunar regions was discovered by Gehrels (1959) and by Teyfel (1959). The present study is the only one that repeats Lyot's work on the whole Moon, and also extends the work to several wavelengths.

##### Development of an Automatic Polarimeter for Measurements of the Integrated Lunar Disk

An automatic polarimeter was designed and developed for measurements of the whole lunar disk. The instrument has two purposes:

to serve as a working model of a design for a prototype instrument for space probes (to Mars, Venus, Jupiter), and to repeat and refine the work of Lyot. The instrument is capable of automatically making simultaneous measurements of the components of an incident electric vector in four planes (separated by  $45^\circ$  from each other) with precisions of 0.1% in degree of polarization. The wavelength range for groundbased work is .32 to .56  $\mu$ . It is capable of operating in a high altitude balloon environment (temperatures to  $-60^\circ$  C, pressure to less than 3 mb) at wavelengths between .20 and .30  $\mu$ . The electronics were designed by P. R. Gray, doctoral candidate in electrical engineering.

### Theory of Operation

Consider a plane, quasi-monochromatic light wave of mean frequency  $\bar{\omega}$  having analytical representations

$$\begin{aligned} E_{||}(\tau) &= a_1(\tau)e^{i[\varphi_1(\tau) - \bar{\omega}\tau]} \\ E_{\perp}(\tau) &= a_2(\tau)e^{i[\varphi_2(\tau) - \bar{\omega}\tau]} \end{aligned} \quad (1)$$

The time varying electric vectors are given by the real parts of the above expressions, where  $a_1$  and  $a_2$  are amplitudes and  $\varphi_1$  and  $\varphi_2$  are phases,

$$\begin{aligned} \text{Re } E_{||}(\tau) &= a_1(\tau)\cos[\varphi_1(\tau) - \bar{\omega}\tau] \\ \text{Re } E_{\perp}(\tau) &= a_2(\tau)\cos[\varphi_2(\tau) - \bar{\omega}\tau] \end{aligned} \quad (2)$$

Analysis of these components in four directions  $0^\circ$ ,  $45^\circ$ ,  $90^\circ$  and  $135^\circ$ , according to Fig. 2, results in the following amplitudes  $A(\theta^\circ, \epsilon)$  where



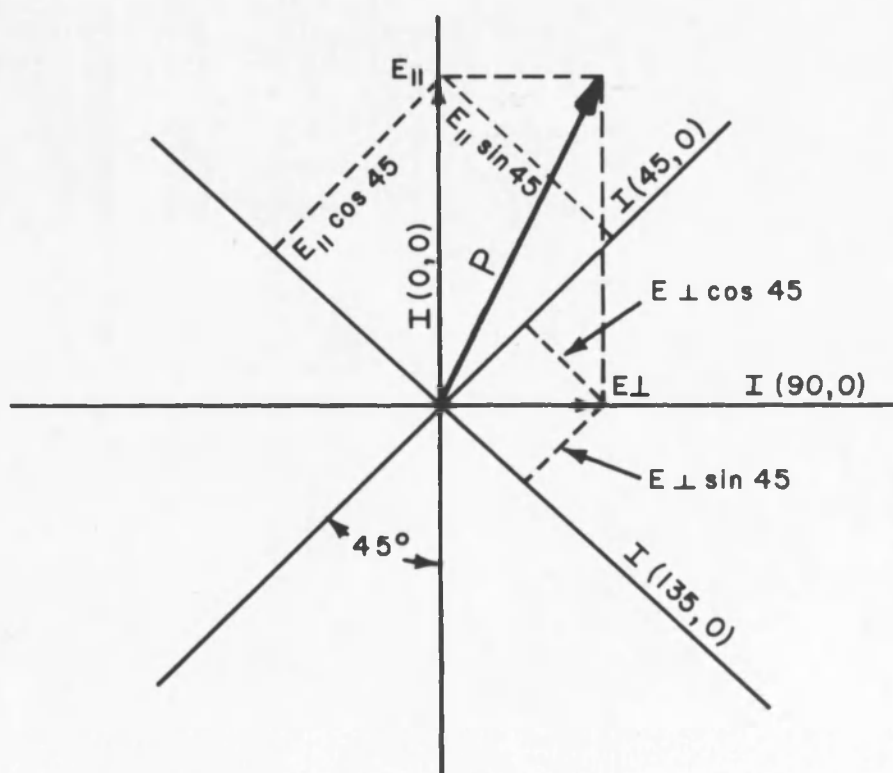


Fig. 2. Analysis of electric vector into four components by two Wollaston prisms.

a general retardance  $\epsilon$  between  $E_1$  and  $E_2$  has been imposed:

$$\begin{aligned}
 A(0^\circ, 0) &= E_{\parallel} \\
 A(90^\circ, 0) &= E_{\perp} \\
 A(90^\circ, \epsilon) &= E_{\perp} e^{i\epsilon} \\
 A(45^\circ, 0) &= E_{\parallel} \cos 45^\circ + E_{\perp} \sin 45^\circ \\
 A(45^\circ, \epsilon) &= E_{\parallel} \cos 45^\circ + E_{\perp} e^{i\epsilon} \sin 45^\circ \\
 A(135^\circ, 0) &= E_{\perp} \cos 45^\circ - E_{\parallel} \sin 45^\circ \\
 A(135^\circ, \epsilon) &= E_{\perp} e^{i\epsilon} \cos 45^\circ - E_{\parallel} \sin 45^\circ.
 \end{aligned} \tag{3}$$

The time-averaged intensities  $\langle A(\theta, \epsilon) A^*(\theta, \epsilon) \rangle$  are, following Born and Wolf (1965),

$$\begin{aligned}
 \langle A(0^\circ, 0) A^*(0^\circ, 0) \rangle &= \langle E_{\parallel} E_{\parallel}^* \rangle \\
 \langle A(90^\circ, 0) A^*(90^\circ, 0) \rangle &= \langle E_{\perp} E_{\perp}^* \rangle \\
 \langle A(45^\circ, 0) A^*(45^\circ, 0) \rangle &= \frac{1}{2} \langle E_{\parallel} E_{\parallel}^* + E_{\perp} E_{\perp}^* + E_{\parallel} E_{\perp}^* + E_{\perp} E_{\parallel}^* \rangle \\
 \langle A(45^\circ, \epsilon) A^*(45^\circ, \epsilon) \rangle &= \frac{1}{2} \langle E_{\parallel} E_{\parallel}^* + E_{\perp} E_{\perp}^* + E_{\perp} E_{\parallel}^* e^{i\epsilon} + E_{\parallel} E_{\perp}^* e^{-i\epsilon} \rangle \\
 \langle A(135^\circ, 0) A^*(135^\circ, 0) \rangle &= \frac{1}{2} \langle E_{\parallel} E_{\parallel}^* + E_{\perp} E_{\perp}^* - E_{\perp} E_{\parallel}^* - E_{\parallel} E_{\perp}^* \rangle \\
 \langle A(135^\circ, \epsilon) A^*(135^\circ, \epsilon) \rangle &= \frac{1}{2} \langle E_{\parallel} E_{\parallel}^* + E_{\perp} E_{\perp}^* - E_{\perp} E_{\parallel}^* e^{i\epsilon} - E_{\parallel} E_{\perp}^* e^{-i\epsilon} \rangle
 \end{aligned} \tag{4}$$

The time-averaged intensities  $\langle A(\theta, \epsilon) A^*(\theta, \epsilon) \rangle$  can be indicated by the symbol  $I(\theta, \epsilon)$ . They are measured by four appropriate orientations  $\theta = 0^\circ, 45^\circ, 90^\circ, 135^\circ$  of an analyzer for linear polarization, and by insertion of a retardance  $\epsilon$  to obtain  $I(\theta, \epsilon)$ . Generally a quarter-wave retarder ( $\epsilon = \pi/2$ ) is used to obtain

$$\langle A(45^\circ, \epsilon) A^*(45^\circ, \epsilon) \rangle \text{ and } \langle A(135^\circ, \epsilon) A^*(135^\circ, \epsilon) \rangle.$$

Substitution of  $\epsilon = \pi/2$ , also of (1) into (4) gives, with  $\varphi_1 - \varphi_2 = \delta$ ,

$$\begin{aligned}
I(0^\circ, 0) &= \langle a_1^2 \rangle \\
I(90^\circ, 0) &= \langle a_2^2 \rangle \\
I(45^\circ, 0) &= \frac{1}{2} \langle a_1^2 + a_2^2 + a_1 a_2 (e^{i\delta} + e^{-i\delta}) \rangle \\
I(45^\circ, \pi/2) &= \frac{1}{2} \langle a_1^2 + a_2^2 + i a_1 a_2 (e^{-i\delta} - e^{i\delta}) \rangle \\
I(135^\circ, 0) &= \frac{1}{2} \langle a_1^2 + a_2^2 - a_1 a_2 (e^{-i\delta} + e^{i\delta}) \rangle \\
I(135^\circ, \pi/2) &= \frac{1}{2} \langle a_1^2 + a_2^2 - i a_1 a_2 (e^{-i\delta} - e^{i\delta}) \rangle .
\end{aligned} \tag{5}$$

The Stokes parameters are defined as

$$\begin{aligned}
I &\equiv \langle a_1^2 \rangle + \langle a_2^2 \rangle \\
Q &\equiv \langle a_1^2 \rangle - \langle a_2^2 \rangle \\
U &\equiv 2 \langle a_1 a_2 \cos \delta \rangle \\
V &\equiv 2 \langle a_1 a_2 \sin \delta \rangle .
\end{aligned} \tag{6}$$

Substitution of the first two quantities of (5) into (6) gives

$$I = I(0^\circ, 0) + I(90^\circ, 0)$$

$$Q = I(0^\circ, 0) - I(90^\circ, 0) .$$

Subtraction of the fifth quantity from the third in (5) gives

$$2 \langle a_1 a_2 \cos \delta \rangle \text{ which } = U .$$

Subtraction of the sixth quantity from the fourth in (5) gives

$$2 \langle a_1 a_2 \sin \delta \rangle \text{ which } = V .$$

Thus the Stokes parameters in terms of our measurable intensities are

$$I = I(0^\circ, 0) + I(90^\circ, 0)$$

$$Q = I(0^\circ, 0) - I(90^\circ, 0)$$

$$U = I(45^\circ, 0) - I(135^\circ, 0)$$

$$V = I(45^\circ, \pi/2) - I(135^\circ, \pi/2) .$$

(7)

The following identity holds

$$\frac{(Q^2 + U^2 + V^2)^{\frac{1}{2}}}{I} = 1$$

for light that is completely polarized. For a light beam consisting of unpolarized and completely polarized parts,

$$P < 1$$

The use of two Wollaston prisms fixed at a mutual angle of  $45^\circ$  allows simultaneous determination of  $I(0^\circ, 0)$ ,  $I(90^\circ, 0)$ ,  $I(45^\circ, 0)$  and  $I(135^\circ, 0)$ .  $I(45^\circ, \pi/2)$  and  $I(135^\circ, \pi/2)$  are measured by inserting a quarter-wave plate before one of the Wollaston prisms. The ellipticity of the light from the Moon and planets has been found to be negligible by Lyot (1929). Lipskii and Pospergelis (1967) report a measurement of  $V \approx 10^{-3}\%$  for lunar regions and the same order of magnitude for rocks with a polarimeter which they claim can detect a  $V$  as small as  $10^{-6}\%$  (1965). For this reason, and for simplicity, only linear polarization is measured here. Therefore,  $V$  is assumed equal to zero, and  $P$  becomes

$$P = \frac{(Q^2 + U^2)^{\frac{1}{2}}}{I}$$

Substituting from (7),

$$P = \sqrt{\frac{[I(0) - I(90)]^2 + [I(45) - I(135)]^2}{I(0) + I(90)}} \quad (8)$$

Simplifying the notation,

$$P = \sqrt{P_{0,90}^2 + P_{45,135}^2} \quad (9)$$

since  $[I(0) + I(90)]$  is the same as  $[I(45) + I(135)]$ .

### Reduction Routine

At an arbitrary orientation  $\psi$ , where  $\psi$  is the angle between the transmission axis of an analyzer and the direction of the maximum electric vector,  $I_1 = P_o \cos^2 \psi$ . We also have  $P = P_o/I_o$ .

An orthogonal analyzer provides  $I_2 = P_o \sin^2 \psi$ . These are for 100% polarized light. When partially polarized light is present the unpolarized component is divided into two equal portions by each analyzer and we have with  $I_o$  equal to the total intensity

$$\begin{aligned} I_1 &= \frac{(I_o - P_o)}{2} + P_o \cos^2 \psi \text{ and,} \\ I_2 &= \frac{(I_o - P_o)}{2} + P_o \sin^2 \psi. \end{aligned} \quad (10)$$

( $I_1$  is perpendicular to  $I_2$  in the Wollaston.)  $P_o$  is the intensity of the polarized component. Thus we have

$$P(0,90) = \frac{I_1 - I_2}{I_1 + I_2},$$

substituting,

$$\begin{aligned} P(0,90) &= \frac{\left[ \frac{1}{2} I_o - P_o/2 + P_o \cos^2 \psi \right] - \left[ \frac{1}{2} I_o - P_o/2 + P_o \sin^2 \psi \right]}{\left[ \frac{1}{2} I_o - P_o/2 + P_o \cos^2 \psi \right] + \left[ \frac{1}{2} I_o - P_o/2 + P_o \sin^2 \psi \right]} = \\ &= \frac{P_o (\cos^2 \psi - \sin^2 \psi)}{I_o - P_o + P_o} = \frac{P_o \cos 2 \psi}{I_o}. \end{aligned}$$

So for one polarimeter

$$P_{(0,90)} = \frac{P_o \cos 2 \psi}{I_o} \quad (11a)$$

and for the polarimeter at  $45^\circ$  to this we get

$$P_{(45,135)} = \frac{P_o \cos 2 (\psi + 45)}{I_o} \quad (11b)$$

These equations are solved simultaneously and used with (9) for the polarization  $P$  and the angle of the electric vector maximum  $\theta$  where  $\psi = \theta + \alpha$ ,  $\alpha$  being the angle that the polarimeter (i.e., one transmission axis) makes with a reference direction (usually taken as the north meridian or the perpendicular to the scattering plane).

#### Optics of the Instrument

The orbital velocity of a spacecraft near a planet requires that observation of a particular area on the planet's disk be made in a very short time in order to be unambiguous. A polarimeter with one Wollaston prism is able to analyze light into the first two Stokes parameters as shown above. It is necessary however to measure the third Stokes parameter  $U$  in order to solve for  $P$  and  $\theta$ . This can be done by rotation of the Wollaston prism and its associated optics through  $45^\circ$  for another measurement -- this time of  $I(45)$  and  $I(135)$ . Because of the finite time required for rotation of the Wollaston and associated optics, and the problems associated with mechanical motion in a high vacuum, it was decided to use two separate Wollastons, the second one fixed at  $45^\circ$  with respect to the first, to accomplish measurements of the parameters in (8) simultaneously. This requires two telescopes.

The optical schematic for each telescope and Wollaston system (polarimeter) is shown in Fig. 3. The first optical element following each telescope is switched into the light beam for one integration and out for a second integration. This element is a pseudo-depolarizer of the type invented by Lyot (1929), and consists of two plates of a birefringent crystal. It has been described by Billings (1951). Each plate is cut with its face parallel to its optical axis, one plate has twice the retardance of the other, and the fast axes of the plates are set at a  $45^\circ$  angle. Thus, each plate is a multiwave chromatic retarder, with the value of retardance  $\rho$  at a single wavelength equal to

$$\rho = \frac{2\pi(n_e - n_o)t}{\lambda} \quad (12)$$

radians.  $t$  is the plate thickness. As a wavetrain propagates through the plate the amount of retardance that one of its components suffers with respect to its orthogonal mate varies with distance travelled.

For each cycle of  $2\pi$  radians retardation all forms and azimuths of polarization are experienced, and at the distance  $t$ , the wave emerges with a specific polarization form determined by  $\rho$ . A wave of different wavelength will emerge with a different polarization form because it suffers a different retardance. Finally, if the bandwidth of wavelengths is large enough a large enough variety of forms will emerge so that the light can not be distinguished from natural light. The magnesium fluoride depolarizers used in the instrument have a retardance equal to  $2400\pi$  radians for light of  $3000\text{ \AA}$  wavelength for the thinner disk and twice this for the thicker.

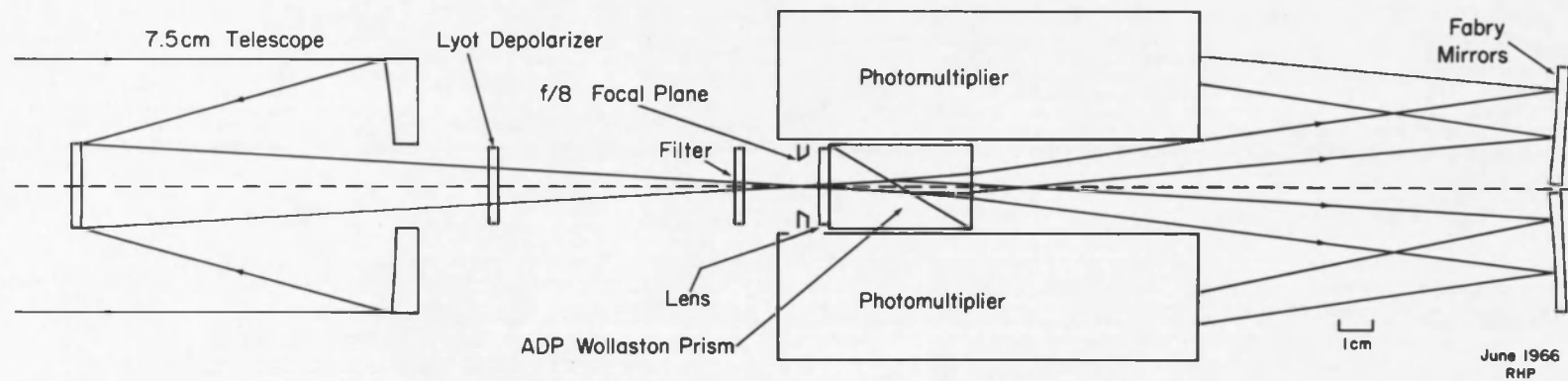


Fig. 3. Optical schematic of polarimeter.



The purpose of the pseudo-depolarizer is to normalize the sensitivities of each photomultiplier to its orthogonal mate in the presence of non-polarized light. The sensitivities over the surface areas of the photomultiplier cathodes are different, the prism transmission is not the same for both beams, and changes caused by flexure or thermal differences would appear as polarization in formula (8). Therefore, in practice the polarization is determined by

$$P = \sqrt{\frac{\left\{ \frac{I(0) - [I(0d)/I(90d)] I(90)}{I(0) + [I(0d)/I(90d)] I(90)} \right\}^2 + \left\{ \frac{I(45) - [I(45d)/I(135d)] I(135)}{I(45) + [I(45d)/I(135d)] I(135)} \right\}^2}{2}} \quad (13)$$

where the intensities containing d are measured with the depolarizers in the beams. These are measured closely in time to the measurements with depolarizer out of the beams so that temporal changes can be assumed negligible. In practice, with 7 second integration and 15 second read-out times, this time interval is approximately 30 seconds. Disks of fused silica are inserted in the beams, when the depolarizers are out, in order to equalize the light losses.

The filters are of such a bandwidth that the depolarizer produces many cycles of retardation over the span of wavelengths; at least 10 cycles are necessary to assure sufficient randomness in the presence of the different bandpass shapes. The focal plane diaphragm selects a fixed size of 1.3 diameter with the f/10 Cassegrain mirror arrangement.

The Wollaston prism is made from ammonium dihydrogen phosphate (ADP) which has a birefringence in the visible of 0.05. It is used

because of its high transmissibility to  $2000 \text{ \AA}$ . The lens contacted to the entrance face of the prism reduces the divergence angle so that the rays will not strike the sides of the prism.

The Fabry mirrors image the entrance pupil (primary mirror of the telescope) onto the photocathodes. This allows the image of the Moon at the focal plane to move without causing motion of the image of the mirror on the (non-uniform) cathode.

Instrumental errors may occur, such as depolarization by scattering from scratches, etc., polarization by incorrectly aluminized mirrors, and incomplete action of the pseudo-depolarizer. These errors are measured as follows. In the first case, measurements of a source shining through several polaroid sheets with their axes parallel (to insure 100% polarization over a large wavelength range) are made with different filters. The polarimeter measures a true polarization of 100.00% as  $99.70\% \pm .05\%$ . Instrumental polarization is determined by observing unpolarized stars brighter than second magnitude (nearer than 40 parsecs) and unpolarized laboratory sources. The instrumental polarization is 0.25%. Since the Stokes parameters for quasimonochromatic light are additive, the appropriate components of (7) for errors are applied additively. See also Gehrels and Teska (1960).

The photomultiplier output currents are fed to current integrators. The polarimeter electronics, designed by P. R. Gray, consist of an automatic observing sequencer and an integrator-gain selector. The sequencer performs the periodic functions of integration, readout, depolarizer out, integration, readout, depolarizer in and filter change,

select gain, integration, etc. The gain selector consists of a voltage comparator which senses the four tube outputs and selects a gain for all four integrators such that none of the integrated voltages will be off-scale. All of the electronics are transistorized, and the polarimeter will operate for several days from +12 and -12 volt automobile batteries. A description of the polarimeter has been published (Pellicori and Gray, 1967).

#### Errors Inherent in the Design

Several sources of error due to the particular optical design used have been recognized. These are discussed briefly.

Because of the short effective focal length ( $f/10$ ) together with its  $f/2$  primary and the 1:3 diameter field of view required, sky light can reach the focal plane directly by passing through the space between the secondary and the primary cutout. This light can be baffled by extending the telescope tube and by increasing the central obscuration with a disk at the back of the secondary. However, when measurements are made on the lunar disk, the comparative sky intensity is only about 0.1%. When it is desired to measure stars or planets the comparative sky contribution is considerable, and poor results are obtained. Even with the elimination of the direct sky light, the sky to sky-plus-star ratio is nearly 0.5 on a first magnitude star and this is sufficiently high to make any star measurements unreliable. Thus, tests for instrumental polarization are made on a bright, unpolarized laboratory sources instead of on stars.

Because of the length of the bidirectional stepping motor used to put the depolarizer into and out of the beams, the depolarizers had to be located close to the telescopes (see Fig. 3). The Fabry mirrors have the purpose of imaging the primary mirrors onto the cathodes. The depolarizers and the fused silica depolarizer-loss simulators are mounted so that they are perpendicular to the telescope beams. They are able to reflect some of the converging beam from the telescope so that an image is formed at a distance to the left in Fig. 3 equal to the focal distance from the depolarizer plane to the focal plane. This image in the space between the primary and secondary is close enough to the primary that an out-of-focus image is transferred to the obscured portion of the telescope images on the cathodes by the Fabry mirrors. Because the depolarizer and its simulator are not co-planar, this image might be present for depolarizer in and not for it out or vice versa. Since the same beam is seen by the Wollaston prisms, identical image conditions exist simultaneously at both cathodes. Therefore, the only way that this can cause errors in the polarization is if the dark (obscured) areas differ in sensitivity so that with one depolarizer position light is present and contributes to the signal but does not for the other depolarizer position. The area of this bright spot is about 1% of the area of the primary mirror image and if the two cathodes have a difference in sensitivity as great as 10%, for instance, the difference between the two tube outputs caused by the presence of the spot in only one of the depolarizer positions is about 0.1% assuming that the areas have equal illuminance. This difficulty can be

considerably reduced by anti-reflection coatings on the depolarizer and its simulator.

### Results

Figure 4 shows the wavelength and phase dependence of the polarization of the integrated disk of the Moon. The letters indicate the five wavelength bandpasses, which are enumerated in Table I. The method for obtaining precision measurements on the Moon was to make 15 to 30 integrations (half the number with depolarizer in and half with it out in alternating sequence) with each of the filters. Since the lunar phase angle changes by about  $12^\circ$  per day, we sometimes observed during early evening and again in the morning before sunrise to get greater phase-angle resolution. The observations were made from Tumamoc Hill, 6 miles west of the campus. Measurements of dark current, which was mostly integrator zero offset and therefore constant, were made at the beginning and end of each filter run. Observations with the five filters took 75 to 100 min., using 7 sec. integration time. Thus, the phase curve of Fig. 4 with five passbands required nearly 4000 integrations. The data were typed by a data printer, and then punched onto computer cards by student assistants. The probable error, a determination consisting of at least 15 measurements, is  $\pm 0.03\%$  polarization. In the presence of dawn or twilight for crescent phases, the probable error has approached  $\pm 0.1\%$  polarization.

Figure 4 includes results from only one of five different lunations studied by the author and Dr. G. V. Coyne. The dashed curve is the data of Lyot averaged over 16 lunations during the years 1922

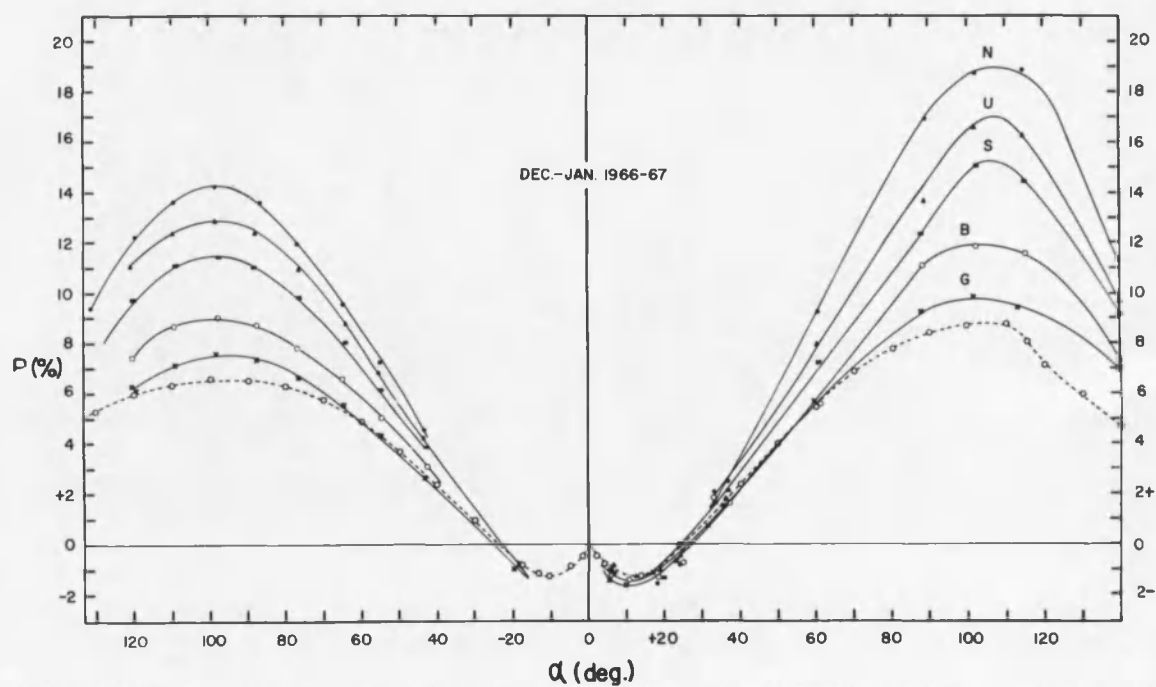


Fig. 4. Polarization vs phase angle for the whole Moon at five wavelengths.

TABLE I. Passband Characteristics<sup>1</sup>

Code <sup>2</sup>	$\lambda_{\text{eff}}$ ( $\mu\text{m}$ )	$1/\lambda_{\text{eff}}$	Eff. Bandwidth ( $\mu\text{m}$ )
N	0.3360*	2.97*	0.0330
U	.3670*	2.72*	.0435
U <sub>m</sub>	.3625	2.76	.0355
S	.3830	2.61	.0250
B	.4490	2.23	.1100
B <sub>m</sub>	.4502	2.22	.0490
G	.5187	1.93	.0915
G <sub>m</sub>	0.5340	1.87	0.0560

\* Averaged over a range of 1.5 to 3.5 airmasses which gives an error of  $\pm 0.03$  in  $1/\lambda_{\text{eff}}$ .

<sup>1</sup> Composed of lunar spectral irradiance, filter transmission, atmospheric absorption, and S-13 response (manufacturer's data).

<sup>2</sup>  $\mu\text{m}$  consists of UG-11 (3 mm) plus BG-12 (2 mm); S of UG-12 (2 mm) plus WG-12 (2 mm); B of GG-15 (2 mm) plus BG-12 (2 mm); G of VG-14 (1 mm) plus GG-14 (3 mm); other filters described in Gehrels<sup>m</sup>, T. and Teska, T. M., 1960, Publ. Astron. Soc. Pac. 72, 115.

to 1927, his effective wavelength (visual) is unknown but it can be assumed to be near  $.55 \mu$ . Thus, since Lyot's effective wavelength is longer than that for the present measures, his polarization is lower. The polarization values are, for the same passband, only four-fifths as great during first quarter as they are during last quarter. This is because there is a greater percentage of maria, which polarize to a greater degree, on the western part of the Moon (last quarter illumination) than there is terrae, see Fig. 5. In a similar way, differences in polarization value at the same passband and phase angle from one lunation to the next which Coyne and the author found (Coyne and Pellicori, 1969) are explained. Displacement of the terminator (meridian dividing the illuminated and non-illuminated portions of the disk) due to lunar libration causes the ratio of illuminated maria to terrae to differ from one lunation to the next. This displacement can be as large as plus or minus  $8^\circ$  over several years. A polarization difference of 2% for  $\lambda = .33 \mu$  and  $\alpha = +87^\circ$  was found between the December 1966 and May 1967 lunations due to this effect. The effect of libration can be seen in the curve of Lyot for positive phase angles  $\alpha$  between  $+110^\circ$  and  $+130^\circ$  (Fig. 4).

The dependence of polarization on wavelength becomes unresolvable for  $\alpha$  between  $-20^\circ$  and  $+20^\circ$ . There is some dependence of  $P$  on  $\lambda$  for the crossover between positive and negative polarization. The phase angle of  $P_M$  decreases systematically with increasing wavelength, being, for example  $+104^\circ$  for  $\lambda = .33 \mu$  and  $+100^\circ$  for  $\lambda = .53 \mu$ . The polarization value decreases again for  $|\alpha| > 120^\circ$  perhaps because



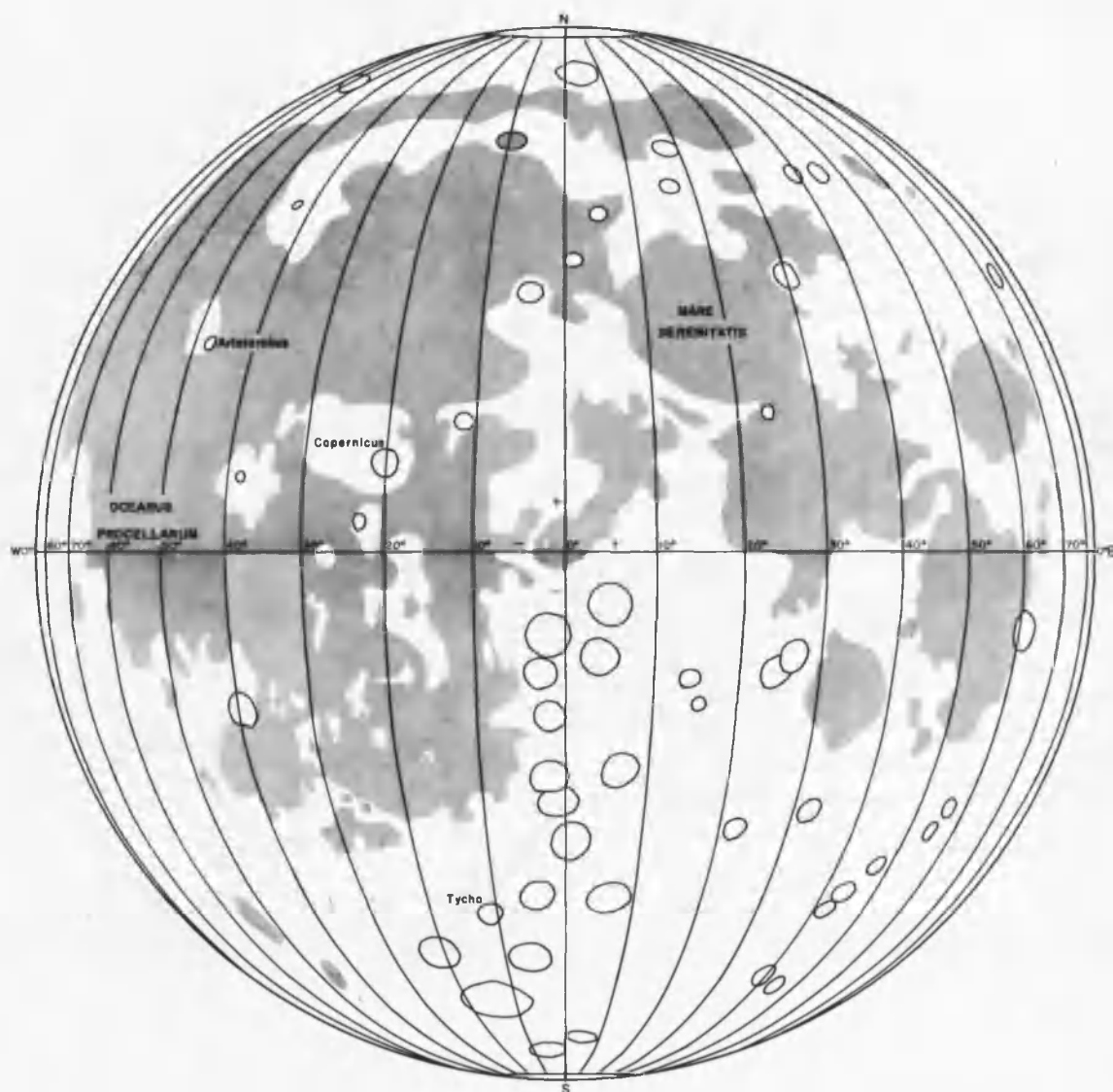


Fig. 5. Distribution of maria and terrae on the lunar disk.

of forward scattering and/or diffraction. It will be seen in Sec. IV that the polarization of mare regions is twice that of the terra regions. Measurements made during the lunar eclipse of 13 April, 1968, revealed a rise in the polarization to a maximum of 2.6% as the Moon entered the umbra. This phenomenon has not yet been explained.

It is reasonable to ask how much is to be learned by study of the integrated light. The data collected in this study has two applications. The first is that the general shape of the curve for the integrated light is the same as that for individual regions (Gehrels, et al., 1964). Secondly, planets and satellites, whose disks we cannot resolve adequately from Earth can be studied in comparison with the Moon. For example, Mercury and Mars, whose disks we can resolve only into large regions, have polarization characteristics similar to that of the Moon. This means that their surface scattering properties are similar. The same conclusion holds for the asteroids except that their crossover points (positive to negative polarization) occur between  $15^\circ$  and  $27^\circ$  instead of at  $23^\circ$  which the Moon shows (Gehrels, et al., 1964). Soon it will be possible to observe the larger satellites of planets like Jupiter and Mars, for example. It can be said immediately, by comparison with the Moon, that Mars, Mercury and perhaps some of the asteroids have surfaces which are similar in texture at microscopic dimensions, and perhaps in composition, to the lunar surface.

## SECTION IV

### COLLECTION OF DATA ON SELECTED LUNAR REGIONS

#### Introduction

Color differences on the lunar surface were suspected as long ago as 1903 (Kruger, 1903). The terrae (i.e., the cratered uplands and mountainous peripheries of the mare basins) were reported to be, in general, redder than the maria. This general conclusion has been confirmed by the photoelectric colorimetry data of van den Bergh (1962), Coyne (1965), McCord (1968) and Pellicori and Mitchell (1969). Some specific exceptions were found by Peacock (1968). The regions observed by Gehrels do not provide a representative sample of mare and terra topographies. For example, of his 13 regions, 8 are mare type, 3 are craters or crater walls but include, for example, Aristarchus which is the bluest region on the Moon, Wood's Region which is very red and Copernicus which is a relatively recent impact crater. The remaining regions include flooded craters or maria with crater rays and ruins. In addition, there can be uncertainties in guiding his 5 arcsec diaphragm in the presence of seeing disturbances (typically 1-2 arcsec), so that unambiguous measurement of a specific terrain type in his regions is subject to doubt. It is not surprising, therefore, that the average difference in B-V of .01 magnitude seen in his data between the maria and terrae is within his error ( $\pm 0.01$  magnitude). The color differences are

graphically emphasized in the composite photography of Whitaker (1965). He combined a negative exposure taken at  $3600 \text{ \AA}$  with a positive taken at  $8600 \text{ \AA}$ ; thus the color contrasts appear as density differences in the composite.

Guided by Whitaker's composites, and Orbiter photographs, examples of maria, cratered highlands, and mountain arcs showing the greatest color contrasts were selected for polarimetric measurements. The topographies chosen were "pure" in the sense that the mare and mountain regions did not include visible craters or rays. The mountains and uplands did not include mare material. The areas were 30 arcsec diameter and are shown in Fig. 6. The passband characteristics are listed in Table I, Sec. III; the narrower filters N, Um, S, Bm and Gm were used. The 61-inch Catalina telescope (stopped to 50 inches to reduce the brightness) was used at  $f/45$ , and observations were restricted to phase angles within  $15^\circ$  of quarter phase in order to measure the polarization maxima. The polarimeter of Gehrels and Teska (1960) was used. In order to intercompare the measurements of maria, highlands, and mountain, it was desirable to minimize the effects of phase angle change with time. The Wollaston prism and phototubes were rotated in six  $30^\circ$  increments about the optical axis. Thus six pairs of orthogonal intensity components were measured which allowed a computer to fit the  $\cos 2 \theta$  curve through the points to find P. The average time elapsed per region with five filters was 30 min., resulting in a change in phase angle of only  $0.1^\circ$ .

## USAF LUNAR REFERENCE MOSAIC

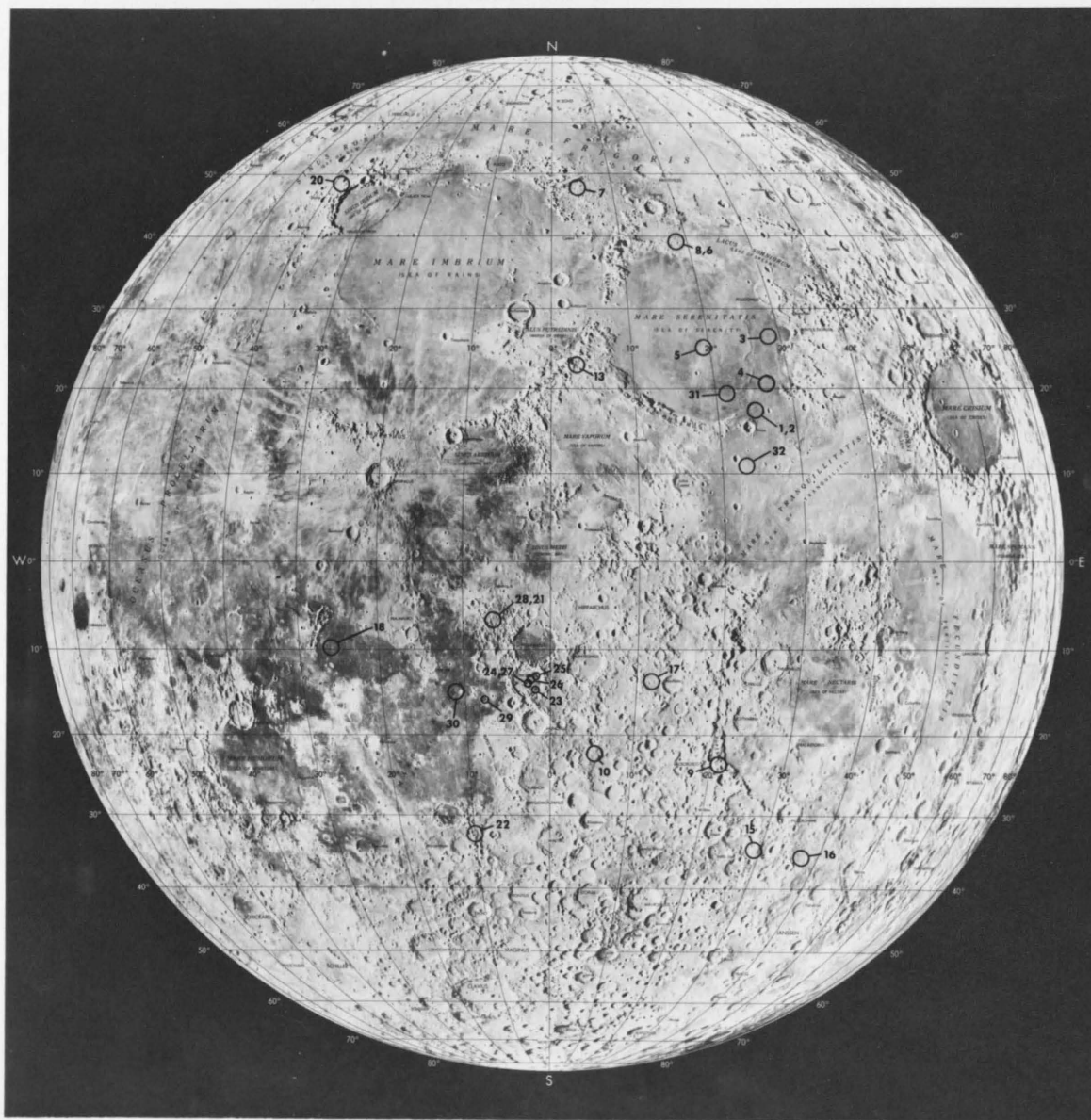


Fig. 6. Location of examples of "pure" topography observed polarimetrically.

### Results

The polarizations are grouped according to phase angle intervals in Table II, Fig. 7 shows averages for the topographic types.

One of the purposes in introducing the filter at  $3830 \text{ \AA}$  was to attempt to detect any anomalies that might occur in the polarization vs wavelength characteristic. Stair and Johnston (1953) reported a dip in the spectral reflectivity of the Moon at  $3830 \text{ \AA}$ . Such a dip should be easily detected as an increase in P at this wavelength (Sec. VI). No such polarization anomaly is found for any of the regions (nor for the integrated Moon). It is therefore doubtful that the spectral reflectivity feature was real.

The first observations, from Summer, 1967, revealed polarizations as high as 28% at  $\alpha = -106^\circ$  and  $\lambda = 3360 \text{ \AA}$  for the darker (bluer) maria, while the redder maria had 26% and the mountains only 15%. It was found that the mountains have up to 2% greater polarization than the cratered uplands. A brightness difference between these topographical types is not detectable in the published photometric data. Thus, the polarimetric measures are very sensitive to topographical differences. Some of these data have been published (Pellicori, 1969).

Some of the first data produced curves having anomalous departures from a monotonic trend. When the regions were remeasured under the same conditions in 1968, these anomalous departures did not reappear. It is concluded (and in most cases verified by notes made during the 1967 observations) that errors in telescope guiding were responsible. The averages for the topographical types, shown in Fig. 7,

TABLE I. Polarizations of Lunar Regions

Region <sup>1</sup>	long. ±10'	lat. ±10'	yr./mo./day U.T. <sup>2</sup> ±.01 <sup>d</sup>	phase <sup>3</sup> ±.08	Polarization at 1/λ (μ)				
					2.98 <sup>4</sup>	2.77	2.62	2.22	1.87
<u>Phase Angle between -106° and -109°</u>									
1. Dark mare near Plinius	+24°00'	+17°00'	7/6/14.14	-107.33	27.93	26.33	24.34	18.08	14.50
2. Dark mare near Plinius	+23 10	+17 00	8/5/4.28	-106.96	26.64	24.39	20.31 <sup>6</sup>	17.28	14.20 <sup>6</sup>
(drift to)	(+23 50)	(+17 00)							
3. Dark mare near Le Monnier	+28 00	+26 30	8/5/4.17	-108.29	30.04	26.96	24.30	19.37	15.83
4. Mare in SE Serenitatis	+26 00	+21 50	8/5/4.20	-107.91	27.64	25.35	22.68	17.66	14.48
5. Mare containing Bessel ray	+19 00	+25 30	7/6/14.18	-106.78	25.86	24.51	21.85	16.01	12.94
6. Mtns. N. of Serenitatis	+18 30	+39 00	8/5/4.13	-108.81	14.21 <sup>6</sup>	12.93	11.60	9.25	7.80
7. Mtn. S. of Vallis Alpes	+ 4 30	+48 00	8/5/4.23	-107.55	12.73	11.80 <sup>6</sup>	10.60 <sup>6</sup>	8.52	7.22
8. Mtns. N. of Serenitatis	+18 30	+39 00	7/6/14.22	-106.32	14.69 <sup>6</sup>	14.80 <sup>6</sup>	14.29	9.99 <sup>7</sup>	8.15
(drift to)	(+23 00)	(+40 00)							
9. Highlands betw. Pons and Fermat	+21 00	-23 30	8/5/4.15	-108.55	10.29 <sup>6</sup>	8.94	7.99	6.44	5.63
10. Highlands betw. Playfair and Donati	+ 6 30	-22 00	8/5/4.25	-107.28	13.28	12.25	10.97 <sup>6</sup>	8.94	7.53
<u>Phase Angle between -92° and -96°</u>									
11. Dark mare near Plinius	+24 00	+17 00	7/6/15.26	- 92.83	25.88	24.44	23.57	17.98	15.79
12. Mare containing Bessel ray	+18 30	+23 30	7/6/15.24	- 93.10	25.81	24.40	23.97*	16.73	13.59

TABLE I. (cont'd)

13.	Apennines betw. Conon and Aratus	+ 3°00'	+23°30'	7/6/15.18	- 93.88	16.67	17.34 <sup>*</sup>	13.23	9.94	8.27
14.	Apennines betw. Conon and Aratus	+ 3 00	+23 00	8/5/5.31	- 94.89	14.23	13.62 <sup>7</sup>	11.86	9.65	8.03
15.	Highlands betw. Stiborius and Rabbi Levi	+29 30	-34 30	7/6/15.15	- 94.20	11.28	10.22	9.67	7.24	6.20
16.	Highlands NW of Brenner	+37 10	-35 50	7/6/15.21	- 93.47	10.43	9.52	8.87	6.78	6.23
17.	Highlands near Albufeda	+11 40	+13 30	8/5/5.29	- 95.16	11.38 <sup>6</sup>	10.69	9.66	7.91	6.79
<u>Phase Angle between +85° and +90°</u>										
18.	Mare surrounding Euclides D	-25 45	- 9 25	8/4/19.44	+ 85.16	30.17	28.04	24.06	16.49	13.75
19.	Dark mare surround- ing Euclides D	-25 45	- 9 25	7/7/29.48	+ 89.04	26.70	24.62	23.01	22.99	14.53
20.	Jura Mtns.	-38 30	+48 00	8/4/19.51	+ 86.00	11.52	11.15 <sup>6</sup>	10.25	7.69	6.86
21.	Highlands NW of Ptolemaeus	- 6 30	- 6 30	8/4/19.48	+ 85.65	13.57	12.71	11.93	8.97	7.83
	(drift to)	(- 8 00)	(- 6 30)							
22.	Highlands betw. Hell and Gauricus	-10 00	-33 00	7/7/29.37	+ 87.75	10.74	11.08	8.92	8.00	7.44
	(drift to)	(-10 00)	(-35 00)							
<u>Alphonsus Features<sup>5</sup> (<math>\lambda</math> and <math>\beta \pm 05'</math>)</u>										
23.	Dark halo-crater SE of peak	- 2 00	-14 15	7/7/28.51	+ 78.46	15.38	---	12.03	9.53	8.50
24.	Central Peak	- 2 40	-13 30	7/7/29.41	+ 88.15	14.60	13.32	12.82	9.21	8.15
25.	Dark halo-crater NE of peak	- 1 35	-12 50	8/5/5.20	- 96.27	14.02	13.36 <sup>6</sup>	12.29	9.63	8.12



TABLE I. (cont'd)

26.	Floor NE of peak	- 2°30'	-13°50'	8/5/5.25	- 95.72	13.66	12.55	11.54	9.02	7.57
27.	Central Peak	- 2 40	-13 30	8/5/5.16	- 96.82	11.60 <sup>6</sup>	10.70 <sup>6</sup>	10.03	7.85 <sup>6</sup>	6.72
<u>Miscellaneous</u>										
28.	Highlands NW of Ptolemaeus	- 6 30	- 6 30	7/7/28.43	+ 77.64	12.56	10.50	10.49	8.18	6.83
	(drift to)	(- 5 45)	(- 8 00)							
29.	Crater Lassell <sup>6</sup>	- 7 50	-15 30	7/7/29.45	+ 88.61	16.12	14.88	13.71 <sup>6</sup>	10.39	8.59
30.	Dark mare incl. Lassell D Nimbus	-11 00	-14 00	7/7/28.47	+ 77.99	19.81	18.31	16.60	13.35	11.21
	(drift to)	(-10 40	(-16 00)							

<sup>1</sup> Type of terrain determined from examination of Orbiter IV photos. Measurements during which drift occurred were included if the terrain type covered was the same as initially intended.

<sup>2</sup> Mid-U.T. of observations for the five filters; year (1967 or 1968), month, day, deviation (.01<sup>d</sup>) includes span from first to last measurement.

<sup>3</sup> Phase angle at mid-time, topocentric to center of crescent; deviation is span from first to last measurement.

<sup>4</sup> Effective wavelength for typical 2 air masses. Extremes are  $1/\lambda=3.00$  (1 air mass) and  $1/\lambda=2.95$  (4 air masses).

<sup>5</sup> 12.4 arcsec diaphragm used for these regions. (29.3 arcsec used for all others).

<sup>6</sup> Probable error:  $.009 \leq \text{p.e.} \leq .014$  times the P(%), all others except for superscript 7 are  $.005 \leq \text{p.e.} \leq .009$ .

<sup>7</sup> Probable error:  $.13 \leq \text{p.e.} \leq .20$  times the P(%).

\* Drift due to guiding error noted during this measurement makes it uncertain.

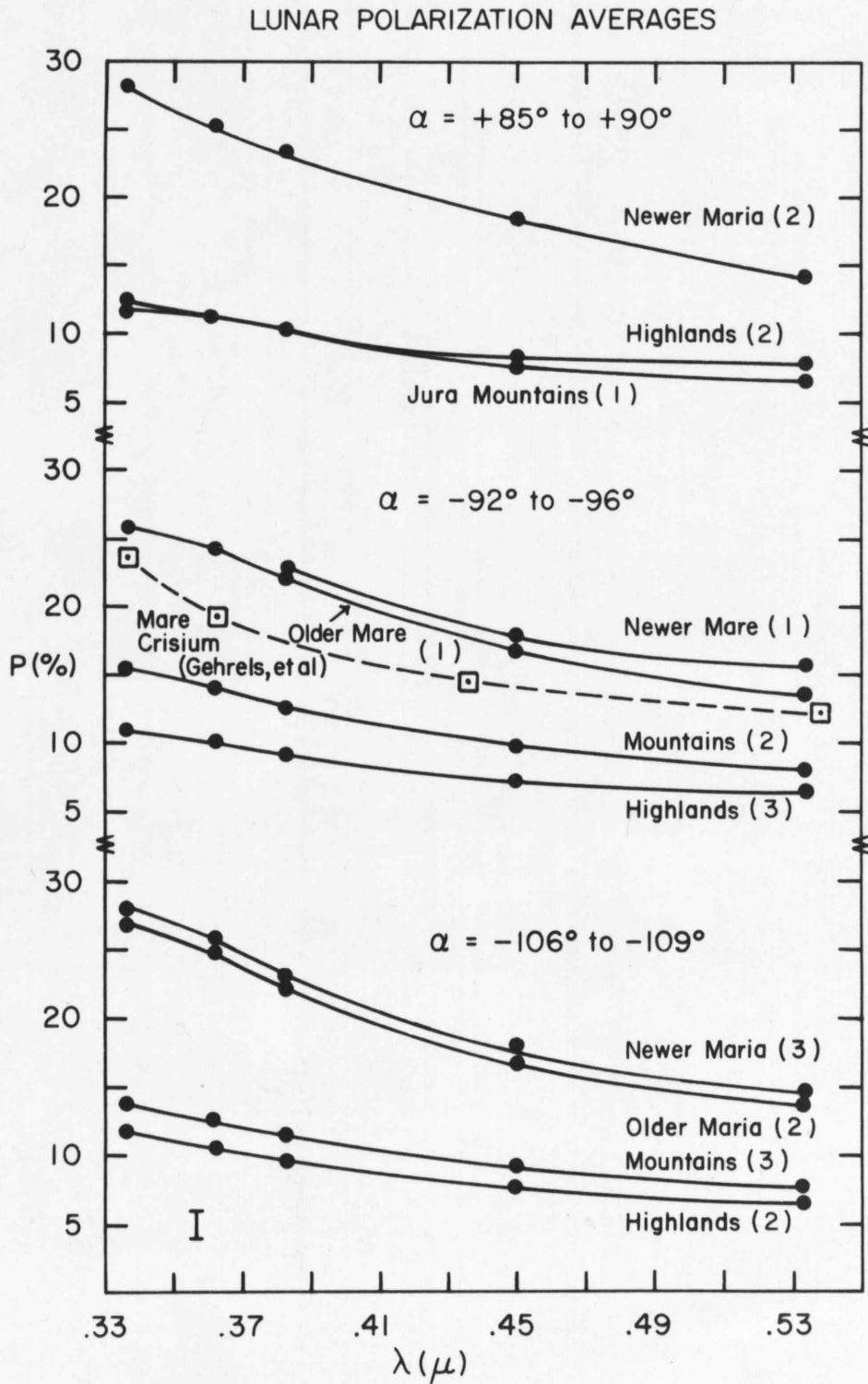


Fig. 7. Average polarization for the various topographical types.

were made after the anomalous features were smoothed out. The vertical bar in the lower left of the figure indicates the maximum deviation from the average curve that the samples showed.

Shown for comparison, in Fig. 7, are the observations by Gehrels on a 5 arcsec region in Mare Crisium using wider filters but the same polarimeter. His region corresponds to the darker (bluer) maria, but occurs in the bright ray field of the crater Proclus. It is, therefore, likely that the region included some unresolved ray material which would account for the lower overall polarization compared with the present measurements on darker (pure) maria.

The averages presented in Fig. 7 are offered as representative data for reference to the polarizations of the topographical types: newer and older maria, cratered uplands (highlands) and mountains. This data will be useful for laboratory comparison research (Sec. VI).

## SECTION V

### ANALYSIS OF THE NEW LUNAR DATA

#### The Polarization vs Brightness Relationship

The data of Sec. IV were averaged according to topographical type for each phase angle group and at each wavelength, and the resulting representative curves are presented in Fig. 6. These averages were then normalized to the data on the newer maria at the wavelength 5340 Å. The resulting curves, after removal of the gross brightness influence, are shown in Fig. 8. Notice that the slope  $dP/d\lambda$  is different for each topographical type, being greatest for the older maria, smaller for the mountains, and least for the highlands (cratered uplands). The older maria have higher polarization at the shorter wavelengths than the newer maria which have higher polarization than the mountains at the same wavelengths. The highlands have comparatively the lowest values at the short wavelengths.

Since the terrae have greater reflectivity for light of longer wavelength than the maria do, it is expected, according to the observation of Provostaye and Desain (1852), reviewed in Sec. II, that the terrae should polarize red light to a lesser degree than the maria do. Conversely, since the maria are bluer (relatively) than the terrae they should polarize blue light to a lesser degree than the terrae do. In Fig. 8 we see that this latter prediction is contradicted by the data because the maria have typically 2 to 4% higher

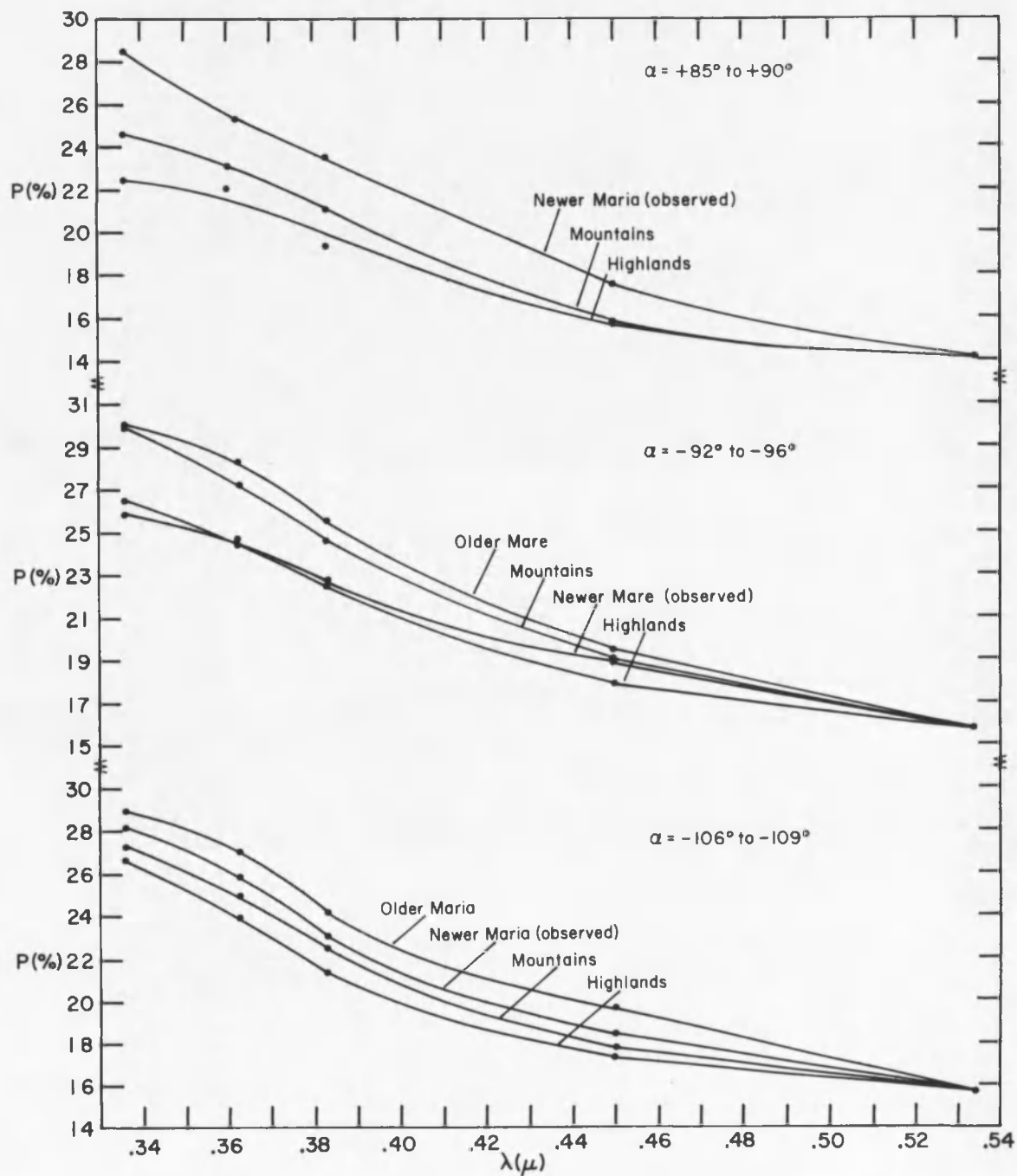


Fig. 8. Average polarization values of the topographical types normalized at  $0.54 \mu\text{m}$ .

polarization of the blue light than the terrae. Apparently, modification of the Provostaye-Desain ("Umov Effect", Sec. II) should be considered.

At this point more knowledge about the polarizing properties of various samples in relation to composition, surface microstructure, particle size, etc. is required (Sec. VI).

## SECTION VI

### LABORATORY POLARIZATION STUDIES ON ROCK AND CHEMICAL POWDERS

#### Introduction

A laboratory investigation of the spectral polarization of solid rock surfaces, powdered volcanic lavas, and some chemicals was carried out to study the polarization mechanisms of these materials and of the lunar surface. As indicated in the Historical Review, Sec. II, there have been many laboratory comparisons with the lunar surface, Lyot (1929) and Dollfus (1962) had made the most progress up to 1960. Lyot had concluded that  $P_M$  and  $\alpha_M$  are independent of refractive index, and that light reflected from the surface of materials shows the negative branch of polarization that Lyot discovered for the Moon. Dollfus found that vitreous surfaces cannot exist on the Moon; that for rough, opaque surfaces, polarization depends on external scattering only, and does not depend on the angle of inclination (this independence was recently confirmed by Coffeen, 1965);  $110^\circ < \alpha_M < 138^\circ$ ; and that the negative branch is reproduced only by "dark grains of all sizes stuck together - grains completely absorbing the light in a few wavelengths of thickness". Dollfus concluded that the lunar surface is made of "small agglomerated opaque grains . . .".

The results of Dollfus were obtained with visible light only. The present work extends the studies over the range 3200 to 6900 Å with 8 narrow-band filters, Table III. Whereas Dollfus's studies

covered the small phase angles as well as near  $90^\circ$ , the present study, because of equipment limitations and because of the potential value of comparison with the precise lunar measurements near  $90^\circ$  made by the author (Sec. VI), is limited to  $\alpha = 90^\circ$ .

Four parameters were varied and their influences on four observed quantities were investigated. The varied parameters were:

1. Particle size
2. Composition
3. Transparency (mean internal optical path length)
4. Surface compaction

and the observed quantities were

1.  $P(\lambda)$  and  $dP/d\lambda$  for  $\alpha = 90^\circ$
2.  $P_M(\alpha)$
3.  $\alpha_M(\lambda = 4035 \text{ \AA}, 6700 \text{ \AA})$
4. Depolarization ( $\lambda$ ) for  $\alpha = 90^\circ$ , where  $D = P_P - P_R$

where  $P_P$  is 100% polarization,  $P_R$  is the polarization remaining after being scattered. It is realized that the transparency is dependent on both the composition and the particle size, and to help separate these dependencies some photomicrography was undertaken using a Leitz Orthoplan. The materials studied, together with the sizes and surface state investigated, are listed in Table IV, where they are classified according to transparency. Except where noted, the surfaces are poured powder, and were prepared by tapping a folded piece of paper, which contained the powder, from a height of about 2 cm above the substrate. The powder fell as loosely agglomerated clumps which



TABLE III. Effective Passband Characteristics  
for Laboratory Work.

Central Wavelength	Bandwidth
0.340 $\mu\text{m}$	0.040 $\mu\text{m}$
.360	.040
.404	.005
.436	.008
.500	.002
.546	.008
.600	.005
.656	.030
.690	.040
0.700	0.006

TABLE IV. Laboratory Polarimetry Samples

No.	Description	Origin	Sizes			Notes <sup>+</sup> , Fig., Surface*, Index
			≤37 μm	37-74 μm	.25-1.5 mm	
A. <u>Semi-Opaque</u>						
1.	Black interior of lava bomb	Hawaii	X	X		depol, Figs. 9,10,13,30
2.	Black <u>aa</u> lava	Sunset Crater, Ariz.	X			Fig. 21
3.	Purple <u>aa</u> lava	Sunset Crater, Ariz.	X			Fig. 21
4.	Vesicular Basalt	?	X		X	Figs. 14,15,16
5.	Olivine Basalt	SP crater, N. Ariz.	X	X	X	Figs. 14,15,16
6.	Pahoehoe lava	Hawaii	X			solid, Fig. 14
7.	Pahoehoe, frothy (Olivine)	Mauna Loa, Hawaii	X	X	X	Figs. 17,19,20,29
8.	<u>aa</u> lava, rust colored	Mauna Loa, Hawaii	X			Figs. 21,23,24
9.	<u>aa</u> lava, purple colored	Mauna Loa, Hawaii	X			solid, Figs. 21,23, 24
10.	Carbon	Chemical	X			depol, Fig. 18
11.	Iron filings (unknown purity)	Chemical	X			depol, micro, Fig. 22
12.	Fe <sub>2</sub> O <sub>3</sub>	Chemical	X			poured, 3.0, pressed, Fig. 22

TABLE IV. (continued)

No.	Description	Origin	Sizes			Notes <sup>+</sup> , Fig., Surface*, Index
			≤37 μm	37-74 μm	.25-1.5 mm	
13.	Carbon + Sulfur	Chemical	X			Fig. 18
14.	Fe <sub>3</sub> O <sub>4</sub> (Magnetite)	Chemical	X			poured, 2.42, Fig. 22
B. <u>Translucent</u>						
15.	Olivine (Mg, Fe) <sub>2</sub> SiO <sub>4</sub>	from Hawaiian sand	X	X		poured, depol, 1.65-1.72, pressed, refl, Figs. 25, 27
16.	CoCl <sub>2</sub>	Chemical	X		X	Fig. 27
17.	Sulfur	Chemical	X			poured, refl, pressed, 1.94 Fig. 26
18.	MgO	Smoked chemical	X			1.74, Fig. 27

<sup>+</sup>photo indicates microscope photographs taken, numbers indicate refractive index. \* Surface textures besides pulverized and poured preparation.

collapsed upon impact with the substrate. This method is to be distinguished from the high-porosity-complex structure of Hapke and Van Horn (1963). Their surface was prepared by allowing particles to fall individually from the sieve and thus electrostatic and inter-particle forces would dominate to build fairy-castle-like structures with interconnected walls and cavities. Both of these surface types have the required porosity to give the shadowing necessary to reproduce the brightness change with phase angle and, in particular, the "opposition effect" i.e., the doubling of the brightness of the Moon as the phase angle decreases from  $5^\circ$  to  $1^\circ$  (Gehrels, et al., 1964). However, the author feels that a surface like the delicate "fairy castle" structure would be considerably modified in the presence of the constant influx of micrometeorites. Photomicrographs of  $\leq 37 \mu\text{m}$  poured surface at  $0^\circ$  and  $55^\circ$  phase angles are shown in Figs. 9 and 10. Note the decrease in detail for  $\alpha = 0^\circ$  due to the absence of shadows.

#### Apparatus

The results were obtained with the apparatus schematized in Fig. 11, which consists of a light source, filter rotatable polarizer, sample holder, depolarizer, and a detector which is on a goniometer housing (Pellicori, Roland, and Teska, 1965). Narrow filters were used; the effective wavelengths and bandwidths as determined by the tungsten lamp, photocathode, and filter are listed in Table III. The polarizer (Polacoat, Inc., 105 UV) was rotated to find the maximum and minimum intensities reflected at  $\alpha = 90^\circ$ . The  $\alpha_M$  (phase angle of  $P_M$ ) was located by rotating the detector and sample by phase angle

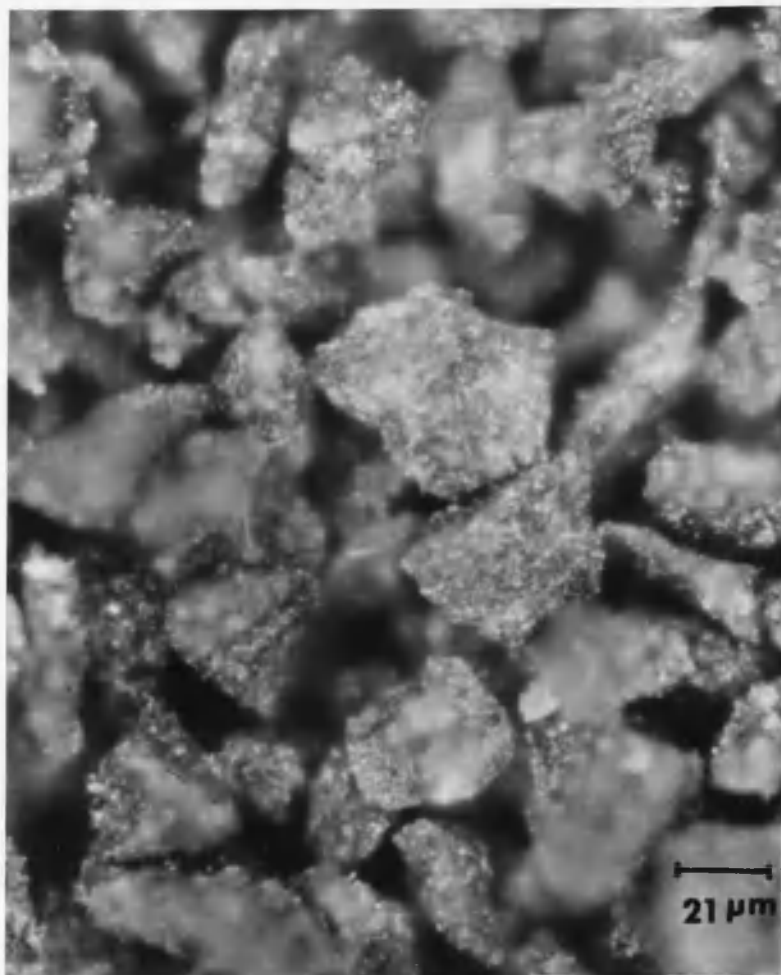


Fig. 9. Photomicrograph of lava powder No. 1, consisting of particles  $\leq 37 \mu\text{m}$  size at phase angle of  $0^\circ$ .

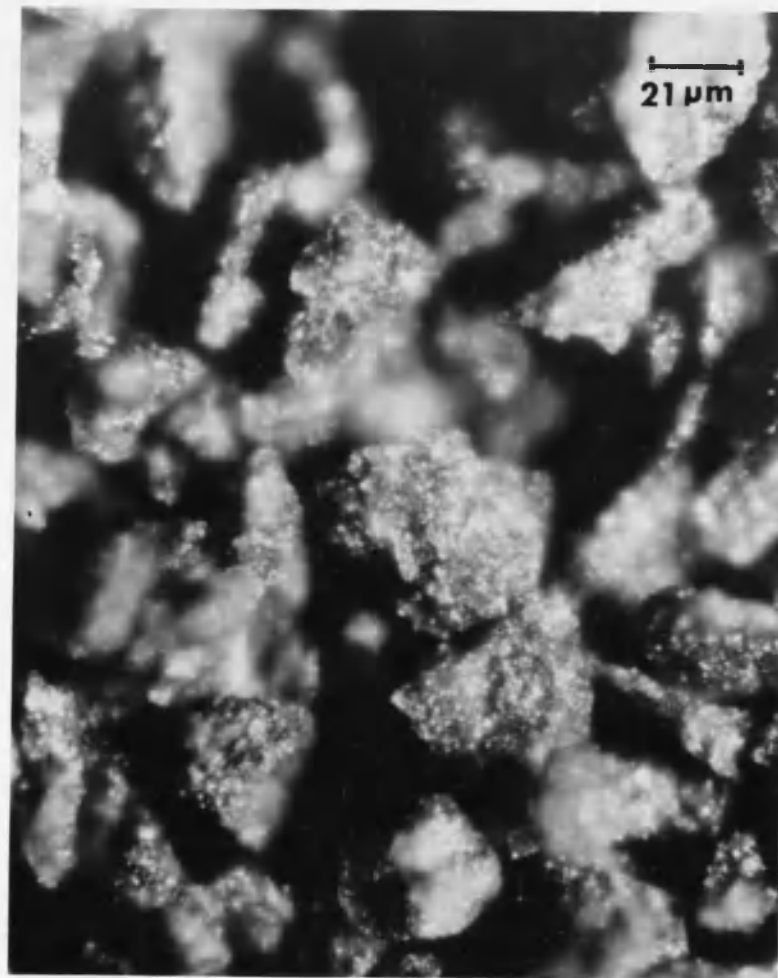


Fig. 10. Photomicrograph of lava powder No. 1 at phase angle  $55^\circ$ .

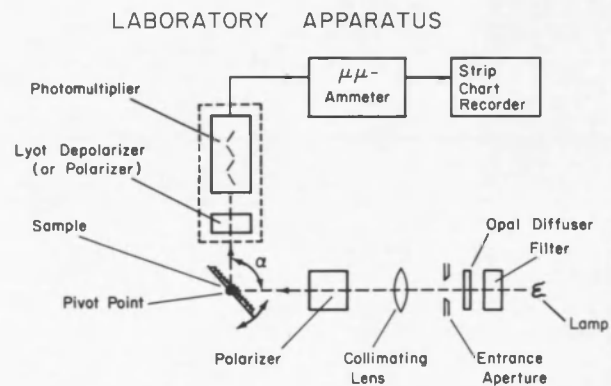


Fig. 11. Schematic representation of laboratory apparatus.

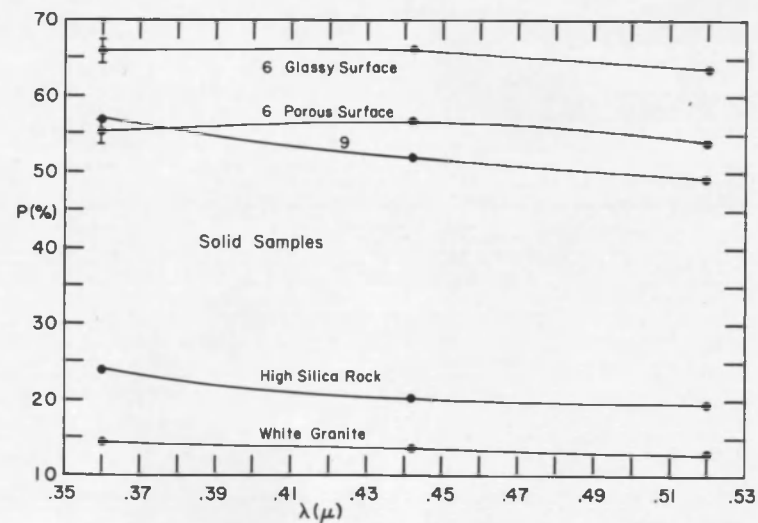


Fig. 12. Polarization vs wavelength for solid surfaces.

increments of  $5^\circ$  or  $10^\circ$  and again determining  $P$ . The lamp light was depolarized by multiple scattering in a piece of opal glass placed before the entrance aperture. The photomultiplier was made polarization insensitive by use of the Lyot-depolarizer before it. The residual polarization ( $\lambda$ ), amounting to 0.5% at  $.33 \mu$  to 1.5% at  $.7 \mu$  was subtracted from the measured  $P(\lambda)$ . (The amount of multiple scattering in opal glass is small at the longer wavelengths). The photomultiplier tube current was detected by a micro-micro-ammeter and read out on a strip chart so that the average signal could be visually separated from the average photon noise. The signal to noise ratio varied from 90:1 to 5:1 depending on the efficiency of the system with wavelength and on the reflectivity of the sample. The signal to noise ratio for carbon, which has a reflectivity of only about 2% was near 5:1, that for olivine, which is bright, was near 100:1. For the powdered lavas, which reflect less than 15%, it was typically 50:1. For all the samples investigated the angle at which the electric vector maximum occurred was  $180^\circ \pm 2^\circ$ , i.e., perpendicular to the plane of scattering (positive  $P$ ). The Moon and some materials give negative  $P$  for  $\alpha$ 's  $< 30^\circ$  (Lyot, 1929), but this range was not studied, as mentioned previously.

#### Lunar Context

A few examples of solid surface and large particle size surfaces (.25 to 1.5 mm) were measured. The polarization is very high, see Fig. 12, and therefore these types of surface are eliminated from comparison with the lunar surface. We know through the direct

photography of the Surveyor soft landers that the particle sizes on the lunar surface are  $< 1$  mm -- which was the limiting resolution of the system. Even the sharpest (most rugged) appearing rocks have smooth edges indicating that they, too, are probably covered with cohesive dust. The conclusion, based on the appearance of dust particles on the solar panels and on the camera viewing mirror (causing appreciable scattered light), is that the particles are on the order of 10 to 50  $\mu\text{m}$  size (Gault, et al., 1967; Hapke 1968). Laboratory work by KenKnight, Rosenberg, and Wehner (1967) and by Egan (1967) point toward sizes  $< 100$   $\mu\text{m}$  (and probably  $< 50$   $\mu\text{m}$ ) required to approach the lunar photometric and polarimetric curves.

For these reasons, most of the present work was done with particle sizes  $\leq 37$   $\mu\text{m}$ , with some samples also measured at sizes 37-74  $\mu\text{m}$  to investigate internal optical path length (IOPL) differences and the contribution by diffraction from smaller particles. The latter size-range particles were washed with Freon to remove particles  $< 37$   $\mu\text{m}$ . This state in the preparation is indicated by (W) in the figures. The rocks were ground with a porcelain mortar and pestle.

The influence of state of compaction was varied by compressing some of the poured samples with a flat surface, or by tapping a poured specimen so that the particles redistributed to form a denser structure.

The materials chosen were mostly varieties of volcanic lavas (basalts) because the Surveyor V, VI, and VII lunar soil analyses indicated a basic (basalt) composition comparable to terrestrial



basalts. In order to have some control over the composition, since volcanic rocks vary in detailed composition, some pure chemicals of known refractive index ( $\text{Fe}_2\text{O}_3$ ,  $\text{MgO}$ ,  $\text{S}$ ,  $\text{CoCl}_2$ ) (some of which are constituents of volcanic sublimate deposits) were measured. These, therefore, can serve as a calibration for the application of polarimetry to remote detection of chemical constituents. This will be discussed again in Sec. VII.

### Results

The data are categorized according to transparency and lava type, and the results are summarized at the end of each list. The results of depolarization experiments are summarized in the Discussion. As before  $\alpha_M$  is the angle for maximum polarization and was generally determined for wavelength 4035 and 6700 Å,  $P$  is the percentage polarization.

#### Opaque Materials

Black inside of bomb. Sample No. 1, Curve Fig. 13, Photo Fig. 9, 10, 31

$P$ : As particle size increases,  $P(\lambda)$  becomes 2 to 3 times greater for sizes  $> 74 \mu\text{m}$ . Little spectral feature, except decrease near 4350 Å and increase at  $\lambda < 4200 \text{ Å}$ . Spectral features are enhanced for smaller particles. Suggests not completely opaque, but some light - especially green and red - escapes while blue and uv are absorbed.

$\alpha_M$ : Is larger for smaller particles, not much dependence on  $\lambda$ .

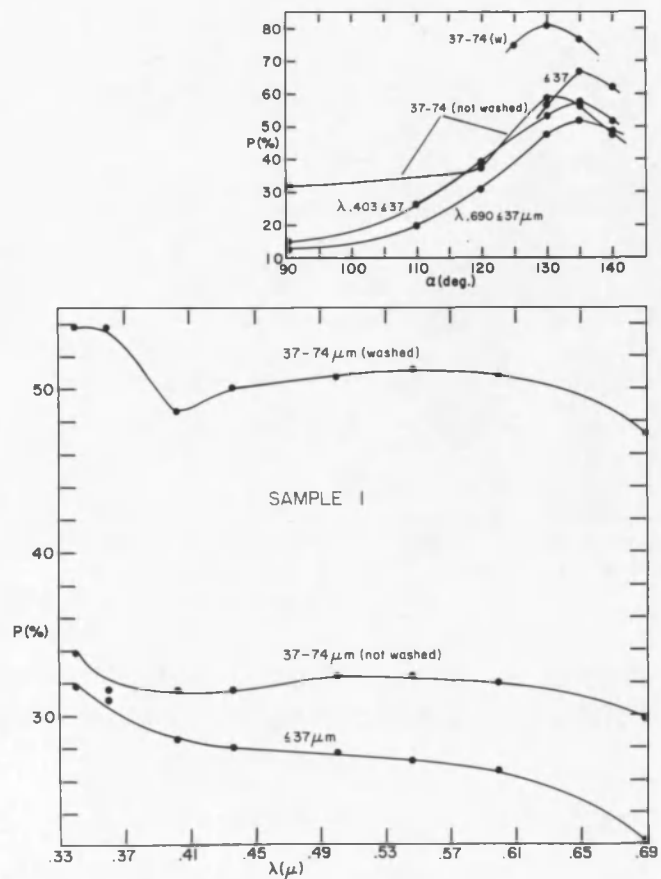


Fig. 13. Polarization of black basalt powder of three sizes, sample No. 1.

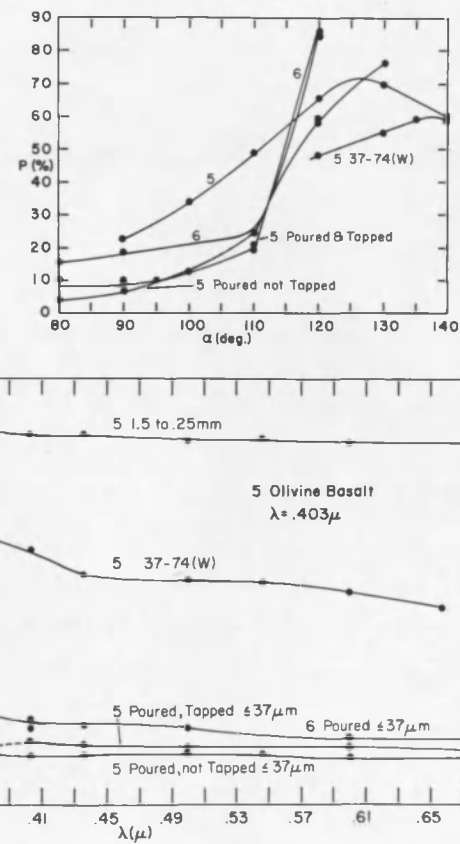


Fig. 14. Polarization of Olivine basalt powder, sample No. 5.

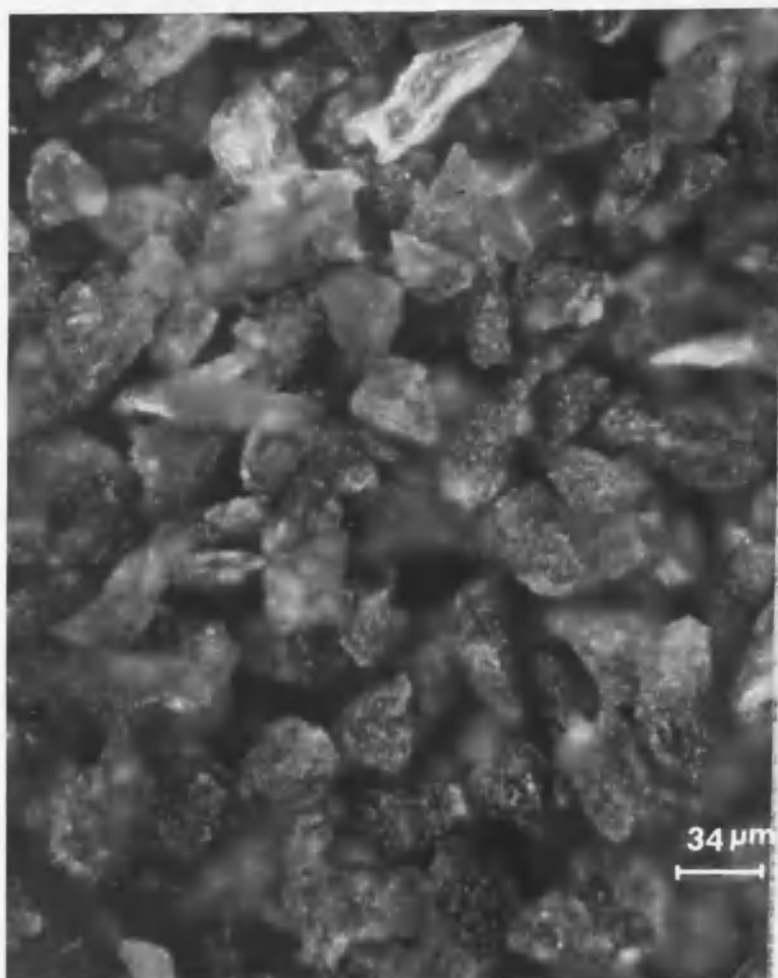


Fig. 15. Olivine basalt, sample No. 5, at 0° phase angle. Size 37-74 μm washed.

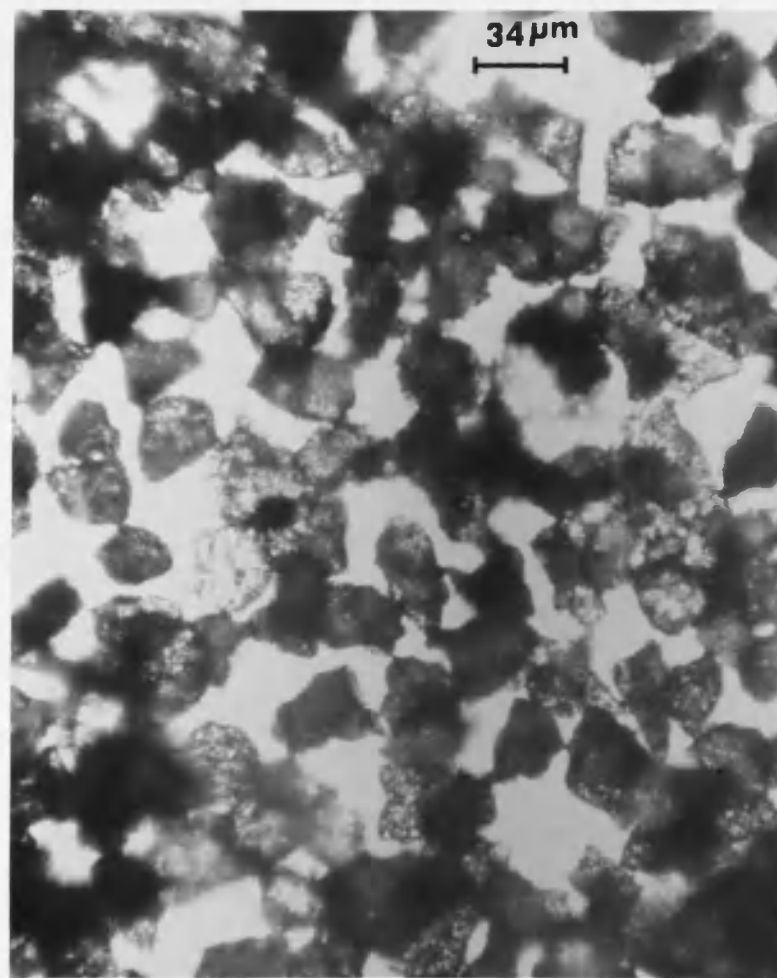


Fig. 16. Olivine basalt, sample No. 5, at 180° phase angle (transmission), size 37-74 μm.

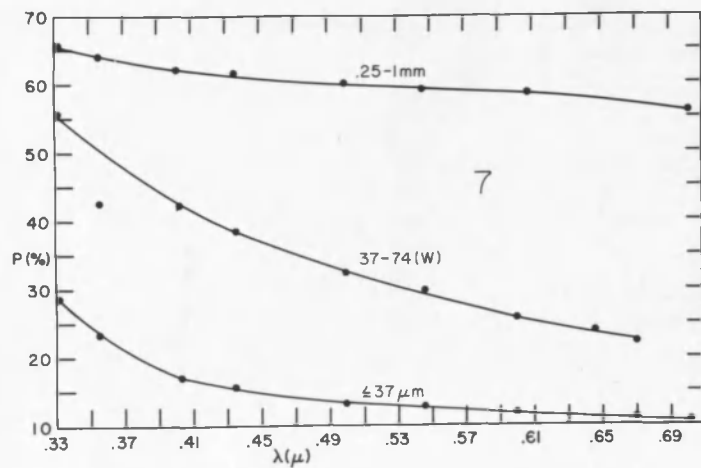
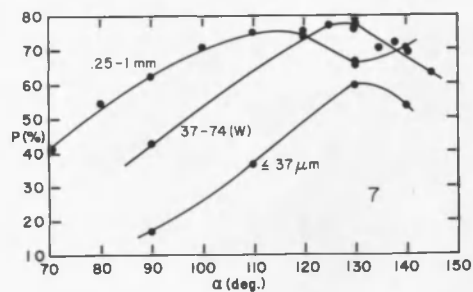


Fig. 17. Polarization of frothy Pahoe-hoe lava, sample No. 7.

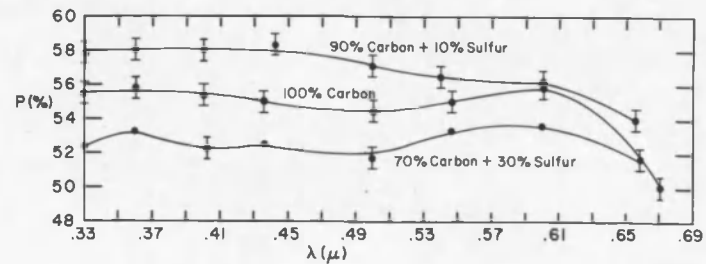
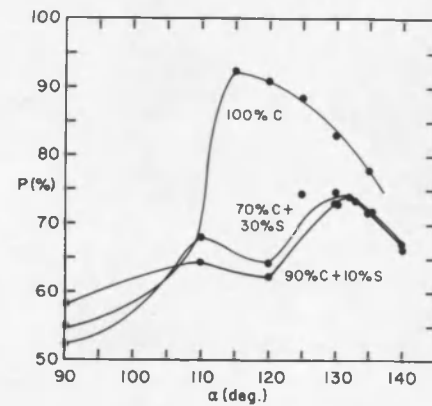


Fig. 18. Polarization of mixtures of carbon and sulfur.

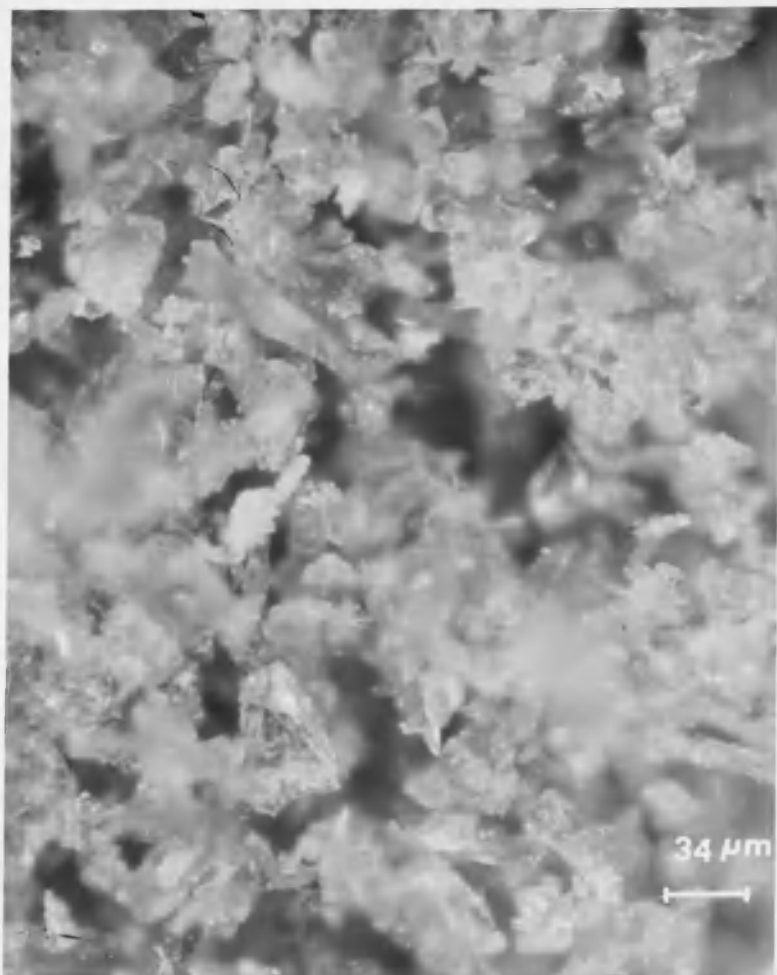


Fig. 19. Sample No. 7, frothy Pahoeohoe basalt at 0° phase angle, size  $\leq 37 \mu\text{m}$ .

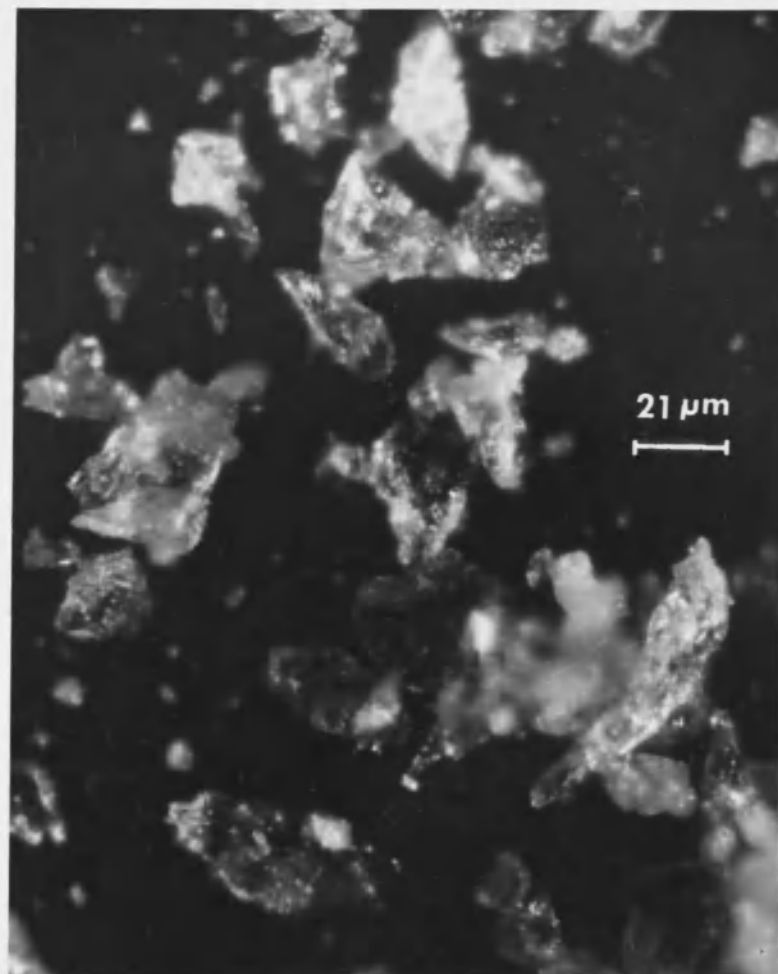


Fig. 20. Sample No. 7, 55° phase angle, sizes  $\leq 37 \mu\text{m}$ .

Vesicular Basalt. Sample No. 4

P: No spectral features except rise at  $\lambda < 4000$ . P for sizes  $\leq 37 \mu$  is  $\sim$  half that for sizes .25-1 mm.

$\alpha_M$ : Occurs at larger angles for smaller size distribution.

Olivine Basalt. Sample No. 5, Fig. 14, photos, Fig. 15, 16

P: For tapped sample, curve shifted up uniformly by 1.5% P because of greater compaction. No spectral features except rise at  $\lambda < 4300 \text{ \AA}$  which is evident even in the .25 to 1 mm size sample.

$\alpha_M$ : No difference between poured and tapped.  $\alpha_M$  occurs at  $127^\circ$  for No. 5 ( $\leq 37 \mu\text{m}$ ), and  $> 135^\circ$  for No. 10. For 37-74  $\mu\text{m}$   $\alpha_M$  is  $\sim 138^\circ$  for No. 5. This is the only reversal of trend seen for the two size distributions.

Pahoehoe. Sample No. 7, Fig. 17, photos, Figs. 19,20,29

P: Rise at  $\lambda < 4900 \text{ \AA}$ . For 37-74  $\mu\text{m}$   $dP/d\lambda$  is large.

$\alpha_M$ : Occurs at larger angle for smaller particles:

$\leq 37 \mu\text{m}$ :  $\sim 130^\circ$ , 37-74  $\mu\text{m}$ :  $125^\circ$ , .25-1 mm:  $110^\circ$ .

Mixture C and S. Sample No. 13, Fig. 18

P: Increases as percentage of S decreases,  $\alpha$  of  $115^\circ$  for C is split into  $\alpha = 110^\circ$  and  $\alpha = 132^\circ$  by only 10% S. ( $\alpha$  sulfur =  $130^\circ$ ). Cannot identify S (e.g.,  $\lambda < 4000 \text{ \AA}$ , 100% S) even for 30% concentration by P( $\lambda$ ) alone.

aa Lavas. Samples 2,3,8,9, Fig. 21, photos, Figs. 23,24

P: The rust colored sample (8) has a greater slope with  $\lambda$  than the purplish. No certain spectral features.

Sample 2 (Sunset Crater) matches Hawaiian purple (9) in P.

$\alpha_M$ : Occurs at larger values for the longer  $\lambda$ 's (by about 2 to 5°). Occurs about the same  $\alpha$  for purple (9) and red (8). Sunset Crater (2), black:  $\alpha_M$  occurs beyond 140° while for others it occurs at  $\alpha$  between 130° and 140°.

Fe. Sample No. 11, Fig. 22

$\alpha = 133^\circ$ .

Fe<sub>2</sub>O<sub>3</sub>. Sample No. 12, Fig. 22. Rust red color.

P: Compacted has 3 times P of poured at  $\lambda < 5700 \text{ \AA}$ , P's equal at  $\lambda > 6000 \text{ \AA}$ .

$\alpha_M$ : For poured occurs at smaller value  $\sim 112^\circ$  for  $4035 \text{ \AA}$  and  $> 130^\circ$  for  $6700 \text{ \AA}$ . For compacted occurs at smaller  $\alpha$ 's ( $\sim 120^\circ$ ) and a second maximum occurs at  $\alpha > 130^\circ$ .

#### General Conclusions on Opaque Samples

P: Rock powders are devoid of spectral features in the range 0.34 to 0.54  $\mu$  except for increase in P for  $\lambda < 4000 \text{ \AA}$  indicating some partial transparency even in sizes up to 1 mm. The highly colored material Fe<sub>2</sub>O<sub>3</sub> is partially transparent in red and P is low there.

$\alpha_M$ : Small dependence of  $\lambda (< 5^\circ)$  except for Fe<sub>2</sub>O<sub>3</sub> (highly colored) where for the highly absorbed light ( $\lambda 4035$ )  $\alpha$  occurs at a smaller value than for the weakly absorbed red light. Little dependence on compaction.

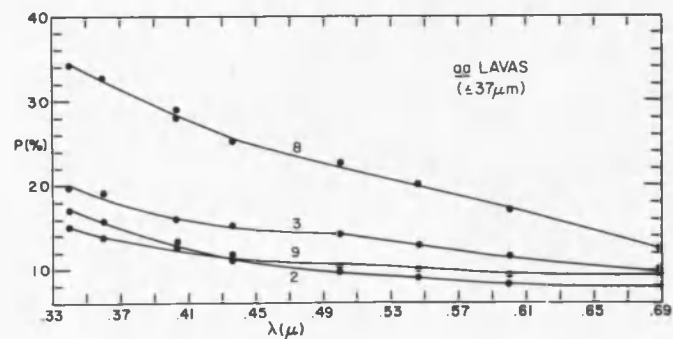
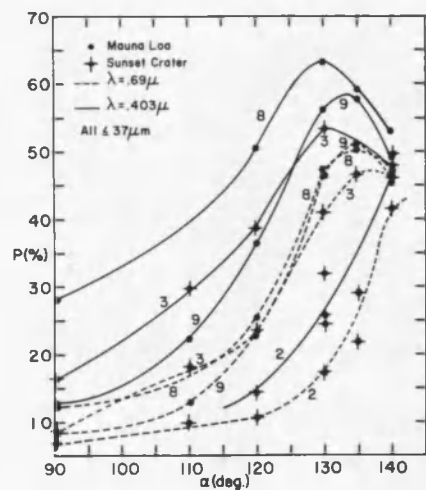


Fig. 21. Polarizations of aa lavas, sizes  $\leq 37 \mu\text{m}$ .

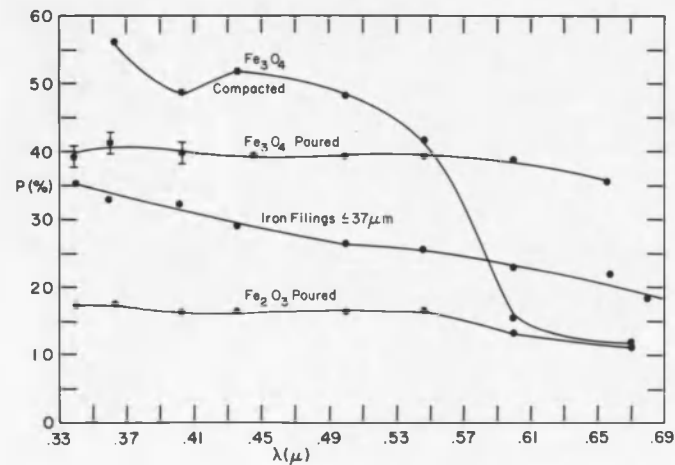
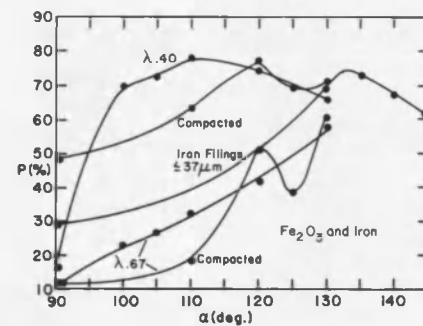


Fig. 22. Polarizations of iron compounds, all  $\leq 37 \mu\text{m}$ .



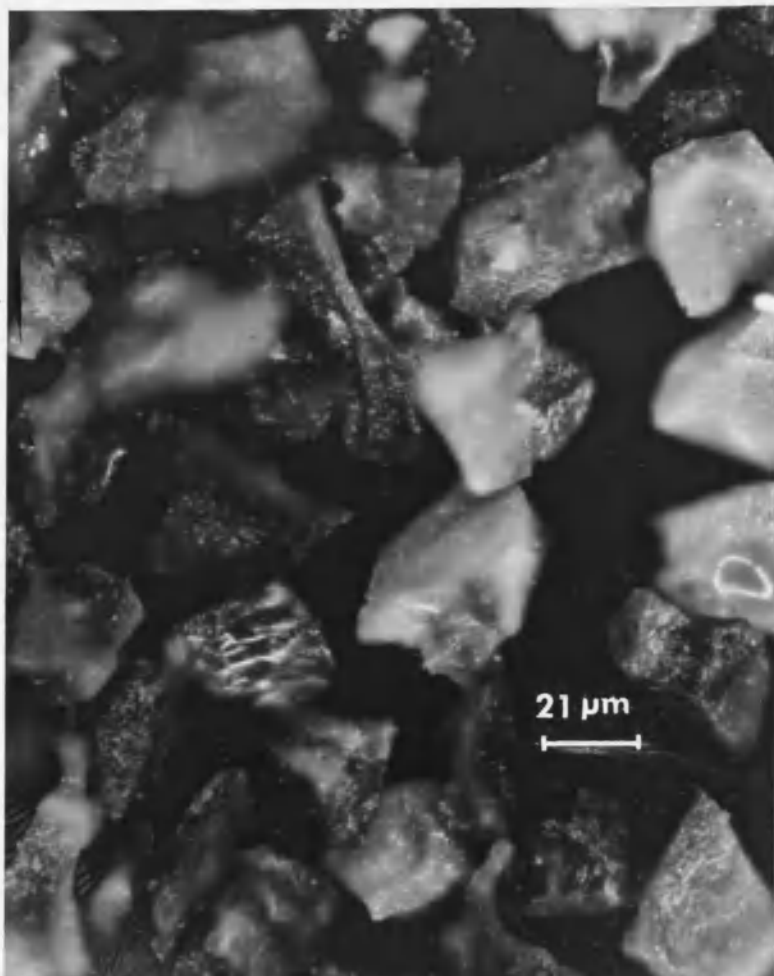


Fig. 23. Photomicrograph of aa lava No. 8,  $0^\circ$  phase angle, size 37-74 μm.

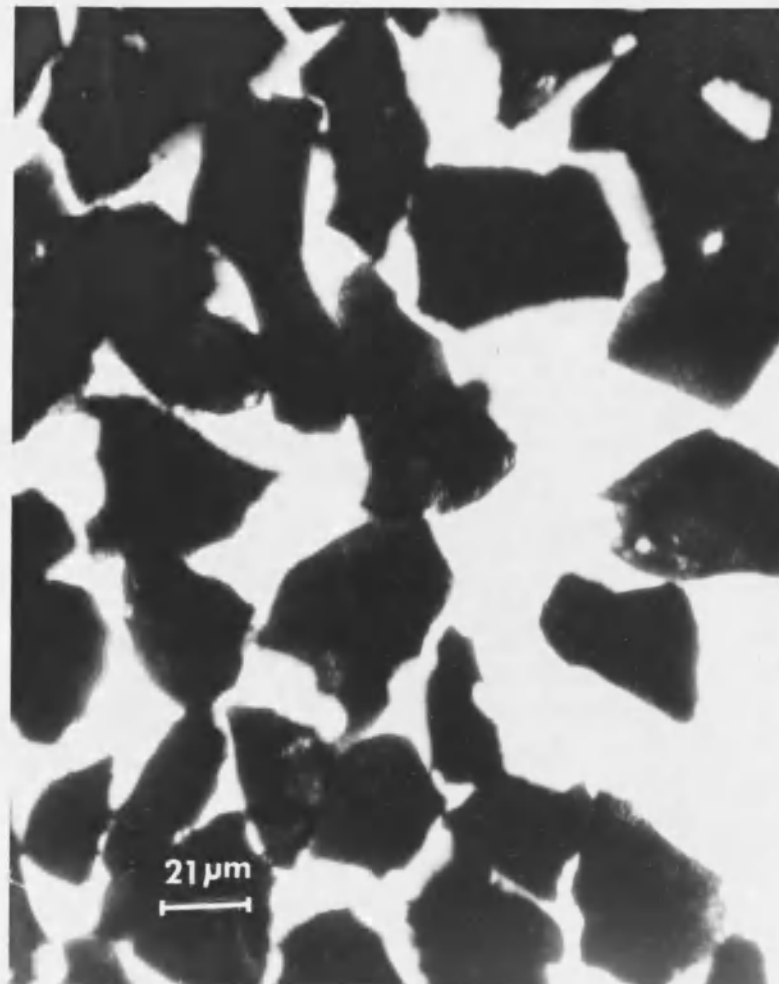


Fig. 24. Aa lava No. 8,  $180^\circ$  phase angle (transmission), size 37-74 μm.

Occurs at larger  $\alpha$ 's for smaller particles. The position angle of the electric vector is always  $180^\circ \pm 3^\circ$  with respect to the plane of scattering.

### Translucent Materials

#### Olivine. Sample No. 15, Fig. 25, photo, Fig. 28

- P: Low P (5%, poured), does not increase much with size except where absorption increasing i.e.,  $\lambda < 4700 \text{ \AA}$  (is yellow-greenish). When pressed is still only 7%.
- $\alpha_M$ : Not a strong function of  $\lambda$ . For larger particles ( $37\text{-}74\mu$ ),  $\alpha_M$  is at smaller angle ( $\sim 138^\circ$ ), for  $\leq 37 \mu$   $\alpha_M > 140^\circ$ . For  $\leq 37 \mu$ , pressed,  $\alpha_M = 127^\circ$ .

#### Sulfur. Sample No. 17, Fig. 26

- P: Low P ( $\leq 5\%$ ) for poured and compacted  $\leq 37 \mu\text{m}$  size except in region of high absorption ( $\lambda < 4300$ ). P for both cases becomes 55% at  $3600 \text{ \AA}$ .
- $\alpha_M$ : For compacted sample  $\alpha_M = 132^\circ$  ( $\lambda 4035$ ),  $\geq 135^\circ$  ( $\lambda 6700$ ). For non-compacted sample,  $\alpha_M \sim 132^\circ$  ( $\lambda 4035$ ) and  $> 140^\circ$  ( $\lambda 6700$ ).

#### CoCl<sub>2</sub>. Sample No. 16, Fig. 27

- P: For large particles (.5 to 1 mm), P is very high in region of high absorption ( $\lambda 3500$  to  $7000 \text{ \AA}$ ). For the violet and red wavelengths which are not so strongly absorbed,  $P < 20\%$ . For sizes  $\leq 37 \mu\text{m}$ ,  $P \leq 15\%$  at region of maximum absorption ( $5500 \text{ \AA}$ ) and  $\sim 5\%$  for violet and red. Powder almost colorless and P relatively uniform

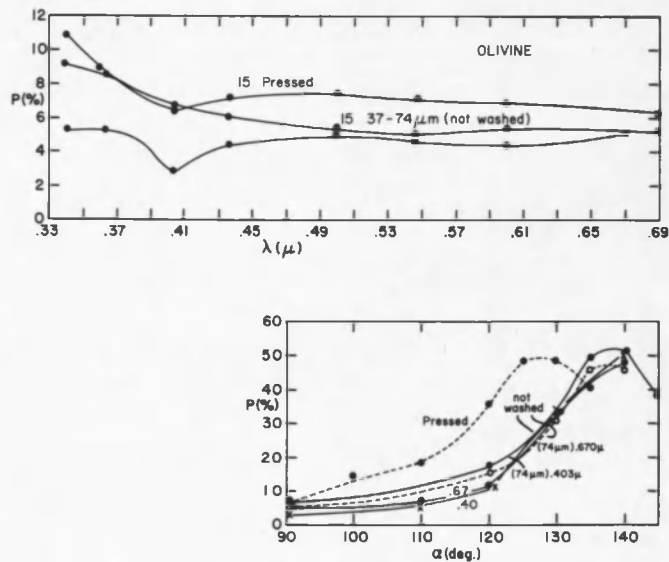


Fig. 25. Olivine, No. 15, size  $\leq 37 \mu\text{m}$  pressed and not pressed, 37-74  $\mu\text{m}$ .

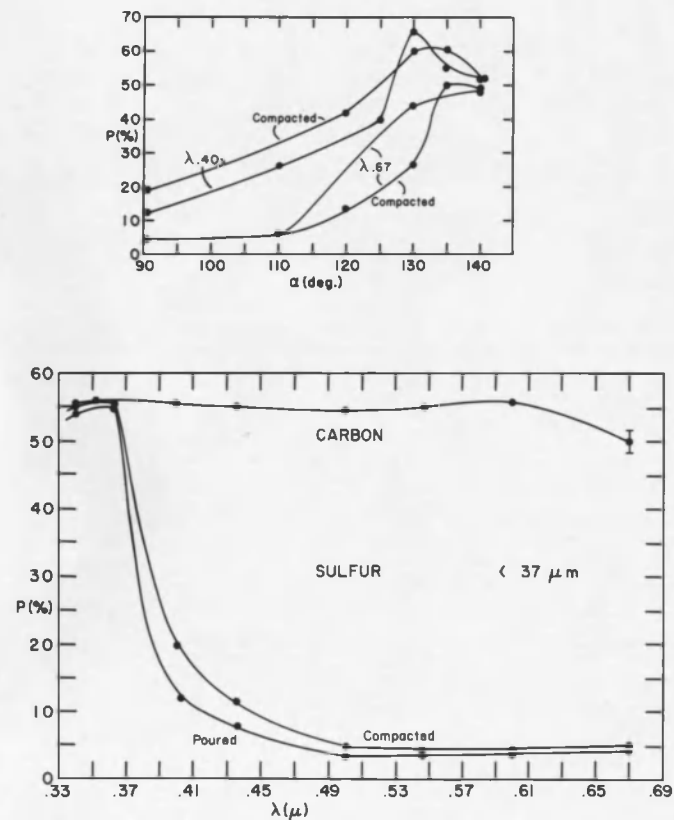


Fig. 26. Sulfur, size  $\leq 37 \mu\text{m}$ , compacted and poured surfaces.

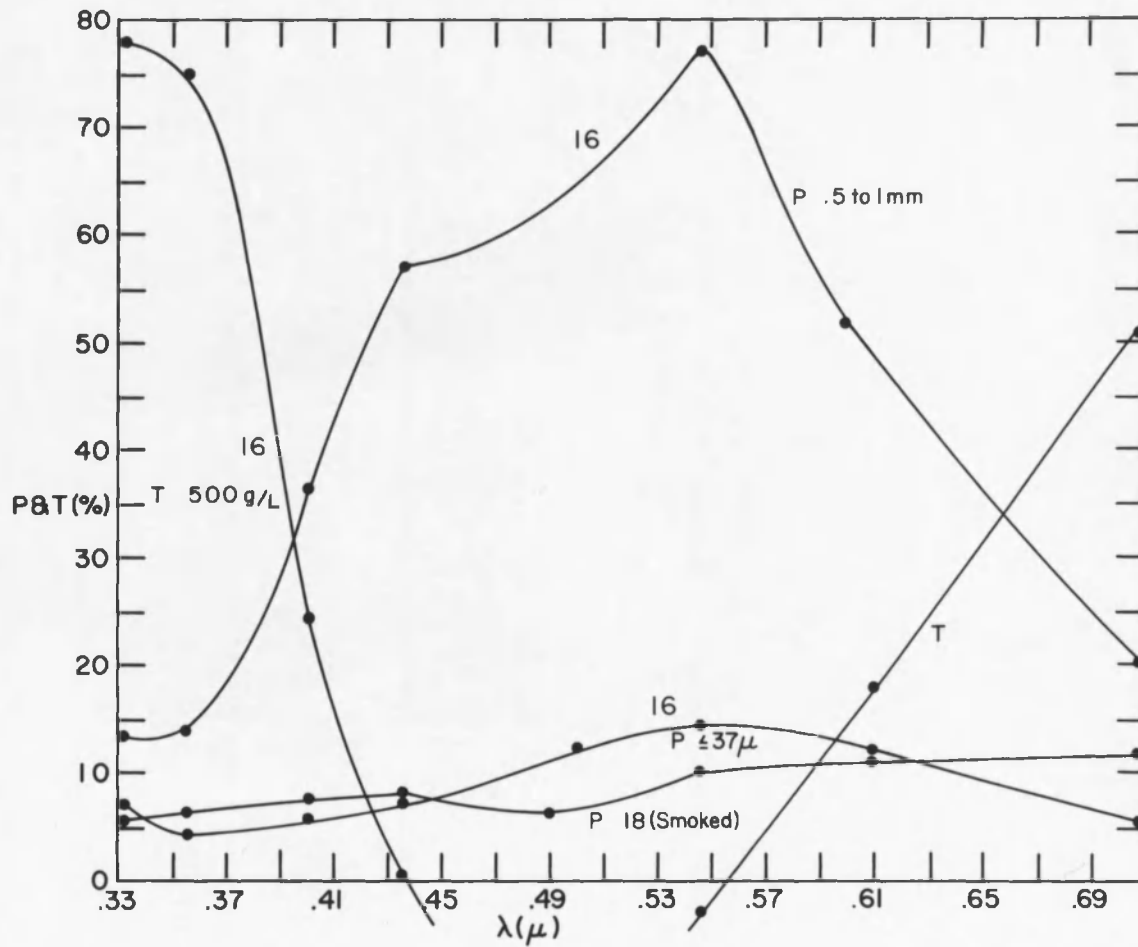


Fig. 27. Cobalt chloride polarization and transmission. Magnesium oxide (smoked) polarization.

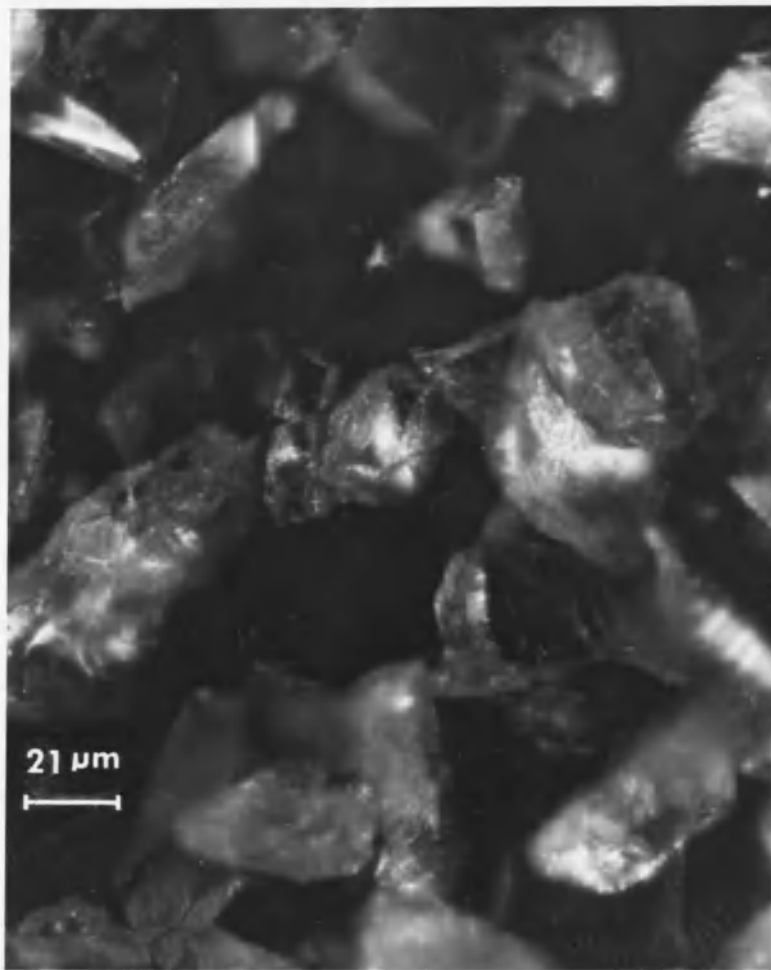


Fig. 28. Olivine, 55° phase angle, 37-74 μm size.



Fig. 29. Frothy Pahoehe, No. 7, 180° phase angle (transmission), 37-74 μm, washed of smaller particles.

with  $\lambda$ , but presence of absorption band still evident.

MgO. Sample No. 18, Fig. 27

P: P is 5 to 12% at 3500 and 7000 Å: almost neutral with  $\lambda$ , and low.

#### General Conclusions on Translucent Samples

P: P is low where the material is highly reflective (and highly transmissive). Where material absorbs (is colored) the P rises. P rises more in the regions of higher absorption as the particle size (optical path length) is increased. Not too much dependence on compaction.  $\alpha_M$  apparently is larger for longer  $\lambda$ 's, for smaller particles, and for lower compaction. All P's are positive and  $P_M = 180^\circ \pm 3^\circ$ . Lunar value never reached.

#### Discussion

##### Polarizing Properties of Materials as a Function of Opacity

We see that in the spectral region where materials are translucent, the light that they scatter has low polarization. If the material has selective absorption (e.g., sulphur,  $\text{Fe}_2\text{O}_3$ , Figs. 26, 22, 27), those wavelengths which are absorbed return high polarization. These facts indicate that light which enters a particle is scattered within the particle and escapes with little polarization or with a random state of polarization. Light of wavelengths which are absorbed within the particle has its polarization determined primarily by external scattering from the surface of the particle and by reflections

from neighboring particles. As a test of this external vs internal mechanism, the depolarizing abilities of opaque (basalt, iron, carbon) and translucent (olivine, sulfur) materials were measured, see Fig. 30. For this experiment a wide angle polarizer was put in place of the depolarizer (Fig. 11), with its transmission axis perpendicular to the plane of scattering. The polarization  $P_r$  was measured as though the polarizer was not there. The phase angle was  $90^\circ$ . If there was no scatterer to depolarize the light, 100% polarization would have been measured. The depolarizing ability  $D$  is indicated by

$$P_p - P_r = D$$

where  $P_p$  is the percentage polarization of the first polarizer in the instrument ( $P_p < 100\%$  for real polarizers),  $P_r$  is the residual polarization with the scatterer in place. It is evident that the translucent olivine is better at depolarizing than the opaque (or nearly opaque) basalt. This indicates that the return of internally scattered light is effective in reducing the net polarization of the light scattered by materials. Furthermore, the smaller particles are more effective at depolarizing than the larger for both opacities. This is due to the small optical path length (OPL) which means more internal light can escape. Also, the increase in depolarizing effectiveness is greater for the  $\leq 37 \mu\text{m}$  olivine particles than it is for the  $\leq 37 \mu\text{m}$  basalt. The size distribution 37 to  $74 \mu\text{m}$  was washed with Freon to remove any small cohering particles that would contribute a diffracted component. The remaining polarizing and/or depolarizing mechanisms are internal scattering and external scattering between large sized

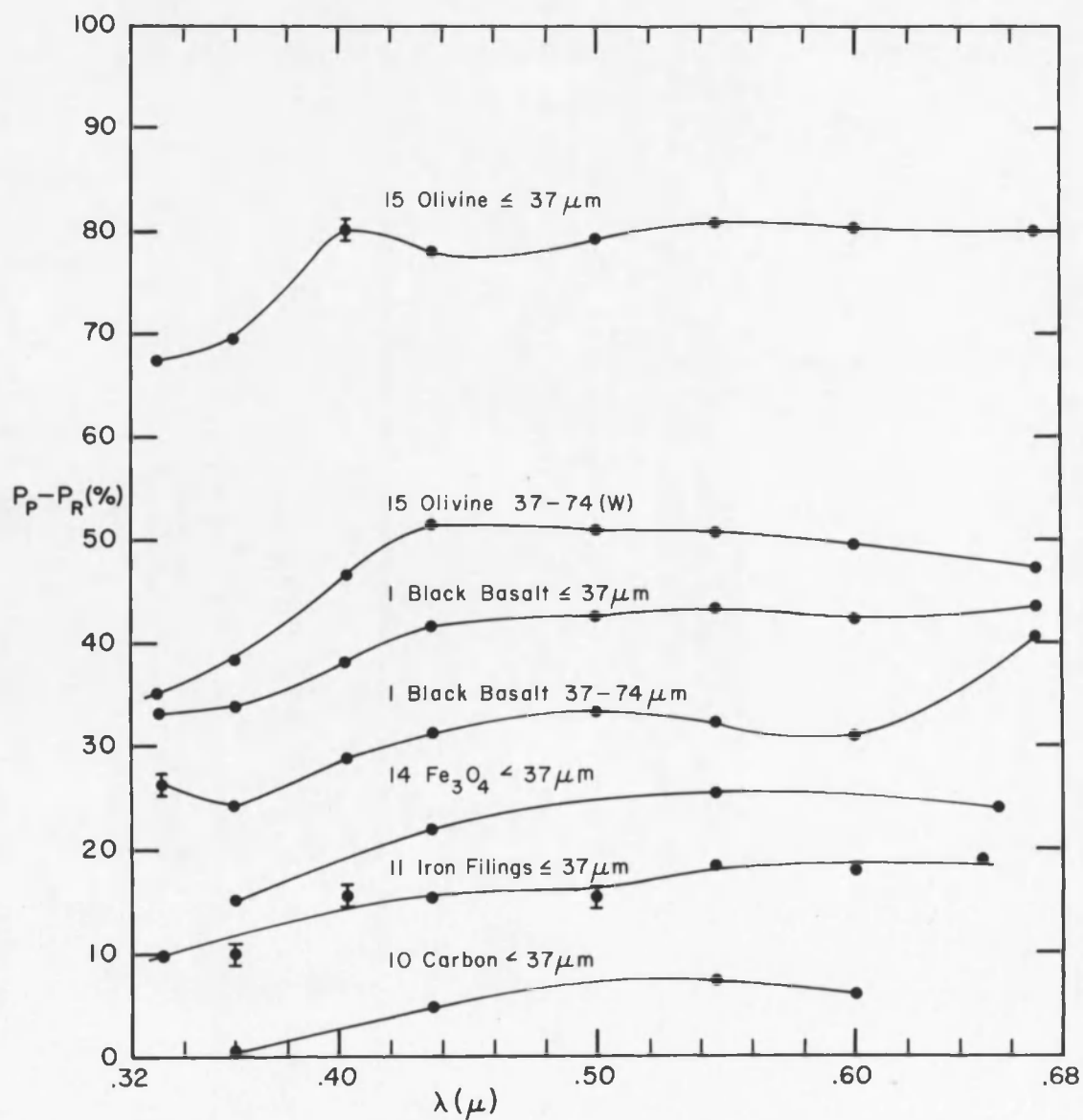


Fig. 30. Depolarizing abilities of translucent and opaque powders as a function of wavelength.



neighboring particles. It is evident from the observations that (a)  $D \neq 0$  for the large basalt particles and that (b)  $P$  increases as the short wavelengths are approached, that this basalt sample is not completely opaque. To eliminate the contribution from internal scattering, the  $D$ 's for carbon and for powdered iron ( $\leq 37 \mu\text{m}$ ) were determined (Fig. 30). The results are  $D = 18\%$  at  $3300 \text{ \AA}$  and  $20\%$  at  $6500 \text{ \AA}$ .  $D$  for carbon  $= 6\%$  and is nearly independent ( $\pm 2.0\%$ ) of  $\lambda$ . Microscopic examination reveals that carbon particles even as small as  $4 \mu\text{m}$  are opaque, while iron particles smaller than  $15 \mu\text{m}$  transmit only approximately 1-2%. Figures 16, 24, 29 and 31 show transmission photographs of some dark lavas. Even the seemingly blackest lava (refl.  $\sim 5\%$ ) is somewhat translucent in sizes  $74 \mu\text{m}$ . That  $D$  is very small, but not equal to zero for the truly opaque materials carbon (and iron), indicates that most of the depolarization is caused by internal transmission and scattering, but that the remainder (5%) is due to external scattering among neighboring grains. The (realistic) materials, e.g., the dark basalts, which approach the lunar reflectivities and polarizations are, in reality, appreciably translucent as we saw from the transmission photographs under high magnification. Note also, that the frothy pahoehoe, No. 7, Fig. 17, the olivine basalt 5, Fig. 15, basalt 1 and aa 8, Fig. 21, which reproduce the lunar polarization in amount also reproduce the  $\Delta P/\Delta\lambda$  of the Moon, see Table V. That  $\Delta P/\Delta\lambda$  increases with decreasing  $\lambda$  for the nearly opaque laboratory samples is taken as evidence, I believe for the first time, that the lunar grains are not completely opaque but are somewhat translucent. An

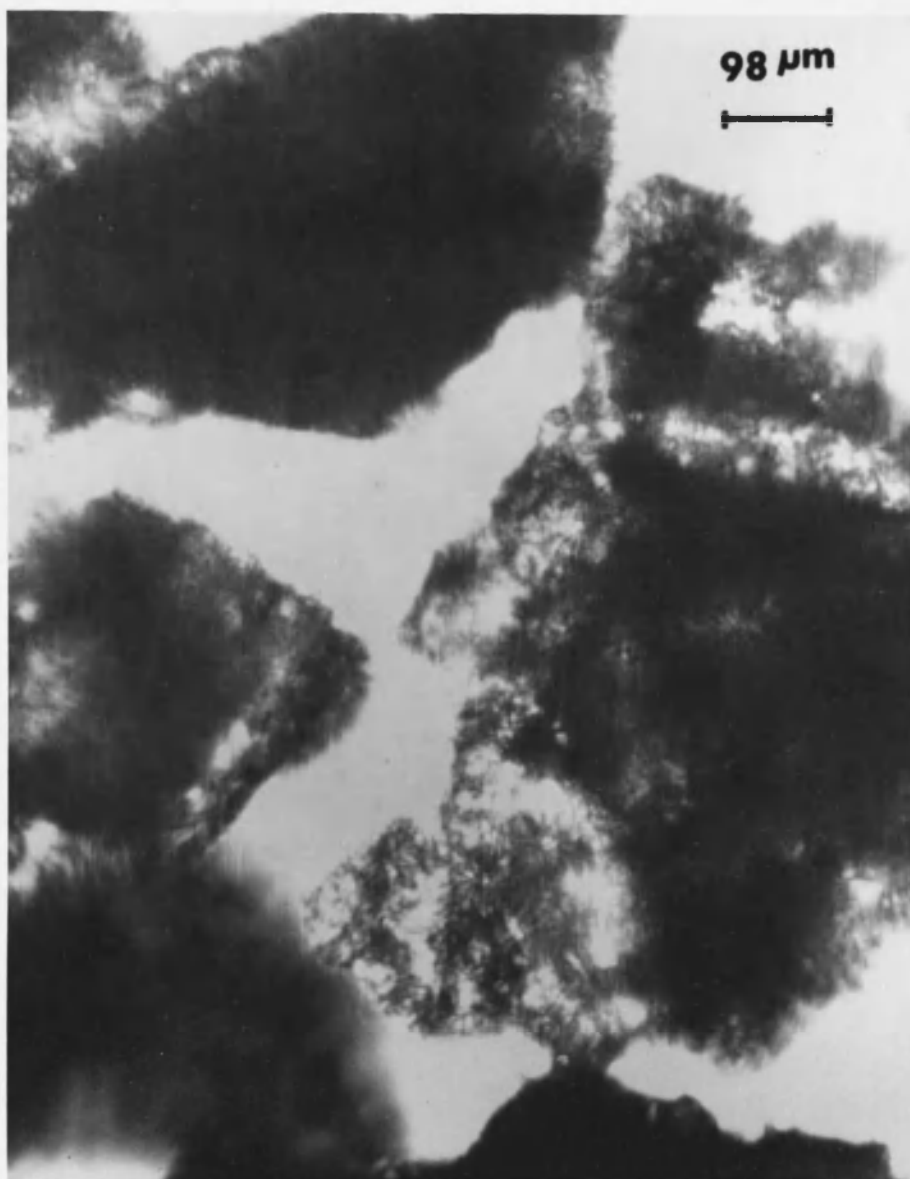


Fig. 31. Black basalt, sample No. 1, 37-74  $\mu\text{m}$  washed of smaller particles,  $180^\circ$  phase angle (transmission).

increase in  $\Delta P/\Delta\lambda$  with decreasing  $\lambda$  is caused by increasing absorption coefficient with decreasing  $\lambda$ . Confirmation of this interpretation was obtained by means of spectrophotometer tracings made on thin sections (6  $\mu\text{m}$ ) of basalts. The transmission decreased by a factor between 1.3 and 4 as the wavelength was decreased from 5000 Å to 3500 Å. These thin sections showed typically < 5% transmittance near 3500 Å per 3  $\mu\text{m}$  thickness.

#### Dependence on Particle Size

It is obvious that, of the particles studied, the larger have higher polarization than the smaller ones. Figure 13 (sample 1) shows curves for 37-74  $\mu\text{m}$  washed and unwashed, and  $\leq 37$   $\mu\text{m}$  size distributions. As the number of small particles is increased the polarization decreases. The dependence of  $P$  on size is lesser for translucent olivine (Fig. 25). The shorter mean internal OPL offered by the smaller particles allows the light that has penetrated and become randomized in polarization state to escape and thus dilute the net polarization. Also, the presence of smaller particles provides more randomly oriented scattering facets to again dilute the polarization. These small sizes also produce some diffraction, which does not change the state of incident polarization, and contributes non-polarized light.

For both transparencies  $\alpha_M$  occurs at larger values for the smaller particles, and does not differ perceptibly between the washed and unwashed 37-74  $\mu\text{m}$  sizes. For all sizes  $\alpha_M$  is at least 20° greater than for the lunar curves.

### Dependence on Surface Compaction

The more compacted the sample is the higher is  $P$ .  $P$  is more strongly dependent on compaction for opaque materials than it is for translucent.  $\alpha_M$  varies irregularly with increased compaction: sometimes increasing (Olivine, Fig. 25), sometimes decreasing (S, Fig. 26,  $\text{Fe}_2\text{O}_3$ , Fig. 22).

The region of  $\alpha_M$  becomes more rounded (less steep). While more highly compacted materials have  $\alpha_M$  that approached the lunar value, they always have excessively high  $P$  and reflectivity.

### Dependence on Composition

We have seen that the more opaque a material is the greater is  $P$ . This is in accord with the interpretation that if the internal optical path length OPL is small enough for light to escape from the interior, the particle will return small polarization. Apparently the major contribution for  $P$  for opaque particles is surface scattering. The structures of the lava particles is revealed by microscopic examination. See Figs. 23, 24 for reddish aa lava No. 8, and Figs. 9, 10 and 31 for black lava No. 1. For the aa, specular reflections are seen (in fact, the illuminating annulus of the objective is imaged by one particle). The lava has differentiated into orange colored, elongated pieces with sharp edges (conchoidal fractures) which appear lighter in the photograph, and into darker, smoother particles. The surfaces of the black lava particles (Figs. 9 and 10) are pitted with minute concave facets about  $1\ \mu\text{m}$  in size. These pits, reflect nearly specularly (the particles look metallic) and probably give rise to the high polarization

from this lava. Notice that the long angular edges present for No. 8 are not present for No. 1. Particle shapes are therefore influenced by composition because hardness and crystal structure depend on composition. Freezing rate -- high for ashes, low for lava flows -- also influences crystal form. The samples of pahoehoe were non-magnetic, while the aa's and the samples 1 through 5 were strongly magnetic.

The suggestion by Dollfus (1962) and by Gehrels, et al (1964) that the Fresnel reflection laws explain the polarization of the lunar surface, and that the "refractive index" can be determined by the Brewster law,

$$\tan \frac{\alpha_M}{2} = n$$

is tested by varying  $n$  and determining  $\alpha_M$  (phase angle for maximum polarization). The results are tabulated for sizes  $\leq 37 \mu\text{m}$ , poured.

No.	Sample	$\alpha_M(4035 \text{ \AA})$	$\alpha_M(6700 \text{ \AA})$	$n_D$	$n_{\text{Calc}}(4035 \text{ \AA})$
10	C	115°	---	2.4	1.57
11	Iron	133°	---	3.0	2.30
12	$\text{Fe}_2\text{O}_3$	110°	>130°	3.0	1.43
14	$\text{Fe}_3\text{O}_4$	140°	---	2.42	2.75
15	Olivine	>140°	>140°	1.65-1.82	>2.8
17	S	130°	~140°	1.94	2.14

No systematic correlation between index and  $\alpha_M$  can be made. Furthermore, increased compaction and/or particle size decreases  $\alpha_M$ , i.e.,  $\alpha_M$  is a strong function of surface compaction. The presence of a material mixed with a different material is detectable in  $\alpha_M$  data: see Fig. 18 for carbon and sulfur mixtures. There it was found that:

Mixture	$\alpha_M$
100% C	115°
90% C + 10% S	~110° and 132°
70% C + 30% S	110° and 130°
100% S	130°

On the other hand, the polarization  $P(\lambda)$  is the same for the carbon mixtures as it is for 100% C. Therefore, the unambiguous identification of a scattering species is not possible by polarimetry alone. However, it is possible to use polarimetry to help confirm and narrow down the possibilities of rock powder constituents. For example, olivine (15) and the black basalt bomb (1) show repeatable dips in their  $P(\lambda)$  curves which should be identifiable with a particular mineral constituent. Similarly, polarimetry in the region 1 to 20  $\mu$  where many igneous rocks have absorption bands (Cruikshank, 1968 and Hovis and Callahan, 1966) should help in the detection of minerals.

Notice that the aa lava No. 2 (Fig. 21) from Sunset Crater, Arizona, has the same  $P(\lambda)$  as the aa No. 9 (Fig. 21) from Mauna Loa, Hawaii.

#### Depolarizing Efficiency

The translucent olivine is better at depolarizing than the black lava according to Fig. 30. For both materials, the smaller sizes depolarize more effectively. Iron filings  $\leq 37 \mu\text{m}$  are less efficient than transparent particles but not nearly as inefficient as the opaque carbon. This confirms the microscope observation that the smaller iron particles ( $<20\mu\text{m}$ ) are, to a lesser extent than carbon, translucent.

The fact that  $D \neq 0$  for carbon (which the microscope reveals as opaque even in sizes as small as  $4 \mu\text{m}$ ) indicates that there is some depolarization due to external scattering. The evidence presented here shows, however, that the dominant depolarizing mechanism is internal scattering within the particle. Note  $D$  for olivine = 80, while  $D$  for carbon = 6.

## SECTION VII

### APPLICATION TO THE INTERPRETATION OF OF LUNAR SURFACE DATA

#### Introduction

The investigations on pulverized opaque and translucent materials reported on in Sec. VI have provided some insight into the polarizing properties of pulverized materials as a function of composition, particle size, degree of compaction, and wavelength near the phase angles of maximum polarization and at  $90^\circ$ . Applications are now made toward the interpretation of the polarizing characteristics of the lunar surface. Comparison with the surfaces of other atmosphereless bodies is also appropriate.

#### The Wavelength Dependence of Polarization

It was demonstrated in Sec. VI that the degree of polarization is not a function of wavelength for totally opaque materials (Fig. 12). On the other hand, polarization increases with decreasing wavelength for the case of translucent materials (Figs. 14, 17, 21). Furthermore, photomicrographs of basalt lavas pulverized to sizes  $\leq 74 \mu\text{m}$  were found to be somewhat translucent (Figs. 16, 24, 29 and 31). These also showed increasing degree of polarization with decreasing wavelength. The slopes,  $dP/d\lambda$ , are comparable to the lunar slopes (Table V). We saw (Fig. 30) that internal scattering is 5 to



15 times more effective at depolarizing than external scattering is. Since absorption coefficients increase with decreasing wavelength, the ratio of the internally scattered (and thereby depolarized) light to the externally scattered (highly polarized) light decreases with decreasing wavelength. It therefore appears that the wavelength dependence of the polarization of the surface of the Moon, and by comparison the surfaces of Mercury, Mars, and asteroids, is explained by the existence of particles which are partially translucent.

The conclusion presented here conflicts with that made by Dollfus (1962), namely, that the particles must be completely absorbing and that the polarization mechanism operating on the Moon is external scattering only. The laboratory investigations by Dollfus (and by Lyot) were made using visual (5500 Å) light, and did not extend to other wavelengths. Therefore, the influence of the (spectral) absorption coefficient was not detected. Furthermore, there is no report that microscopic examination was made in order to detect translucency.

#### Reproduction of the Lunar Phase Angle of Polarization Maximum

While it was possible, as discussed above, to reproduce the  $dP/d\lambda$  of the Moon with several pulverized basalt surfaces (Table V), none of the samples had a phase angle of polarization maximum,  $\alpha_M$ , approaching the lunar value of  $105^\circ$ . The values were always greater than  $125^\circ$ . Increasing the particle size decreased  $\alpha_M$ , but, at the same time, increased the degree of polarization to beyond the lunar value.

Coffeen (1965) reproduced the  $\alpha_M$  and the entire lunar curve with fairy castle surfaces of powdered volcanic cinders of sizes

TABLE V. Lunar and Laboratory Values of  $dP/d\lambda$  for  $.33 \leq \lambda \leq .43 \mu$ ,  $\alpha \approx 90^\circ$ , and Two Size Distributions.

Lunar regions		$dP/d\lambda$	
Average mare		.9	
Average terra		.4	
Laboratory samples*		Sample No.	$dP/d\lambda$
			$37-74\mu m$
			$\leq 37\mu m$
Frothy Pahoehoe		7	1.7
Black basalt bomb		1	~.4
aa lavas		2	.5
"		3	.5
"		8	.6
"		9	.9
"			.7

\*Origins: 1, 7, 8, 9 Mauna Loa, Hawaii; 2, 3 Sunset Crater, Arizona.

$\leq 37 \mu\text{m}$ . Egan, et al. (1966) reproduced all the lunar polarimetric and photometric characteristics with a surface consisting of millimeter sized chunks of a volcanic ash dusted with  $1 \mu\text{m}$  particles of itself. The  $1 \mu\text{m}$  particles decreased the relatively high polarization that the large chunks gave, and in this way a surface reproducing the lunar values was manufactured. On the basis of the Surveyor photography, Egan's model is of questionable applicability to the Moon because millimeter sized pieces would have been resolved if they existed in abundance. Instead, the Surveyor photography indicated, as discussed in Sec. I, that the abundance of particles must be less than  $100 \mu\text{m}$  in size (Gault, et al., 1967). The Egan model works because the  $1 \mu\text{m}$  particles are highly translucent, and thus internal scattering contributes a large amount of unpolarized light. Also a large diffracted component, which would be unpolarized, would be contributed by these small sizes.

An important differentiation that occurs between volcanic products was pointed out to me by Dr. W. K. Hartmann. Magma which has cooled quickly, for example, ashes and cinders, forms small (1 to 5 mm) glassy particles; that which has cooled slowly, for example, massive lava flows, has large crystals. Lyot, Coffeen and Egan, et al., were able to reproduce the lunar characteristics using volcanic ashes or cinders. The volcanic samples in the present study fall into the category of slowly-cooled material. It is reasonable to expect that the differences in crystal size and also in mineralogy due to the cooling rate will affect the specific optical properties of the samples. A lunar surface composed of a pulverized lava flow might have different

optical properties than one composed of ashen particles. Lyot studied both ashes and lavas; however, he did not control either the particle sizes or the surface structure. They are, in fact, unspecified in 80% of his samples (Lyot, 1929). Examination of his data, with due appreciation to the above shortcoming, reveals no systematic differences in the angles of maximum or minimum (negative) polarization. There is a suggestion that the crossover angle between positive and negative polarization might be about 4 degrees smaller for the powdered lavas than for ashes. Perhaps the reason why the present work found all  $\alpha_M$ 's to be larger than the lunar values is due to the above mentioned differences in the samples studied.

#### Identification of Lunar Materials Through Phase Angle of Maximum Polarization

Section VI indicates that it is not possible to distinguish materials on the basis of their  $\alpha_M$  because this phase angle is not a systematic function of refractive index, but depends on particle sizes and surface microstructure. Features in the spectral polarization curve (e.g., Fig. 25) may, however, be useful in suggesting compositions. A polarimetric reconnaissance with good spectral resolution, as with narrow filters similar to those used in the present laboratory study, over a wide spectral baseline should be made on small regions (5 arcsec).

Typical examples of such a region are Aristarchus, Tycho, Wood's region, dark halo craters (Alphonsus), bright recent rays, etc.

### Differences Between the Maria and Terrae

In Sec. V, Fig. 8, observational evidence was presented showing that  $P(\lambda)$  (polarization dependence on wavelength) is different for the topographical types. The maria have greater polarization at the shorter wavelengths than the terrae. The laboratory results (Sec. VI) indicated two characteristics of a pulverized surface that determine, predominantly, its polarizing properties. They are particle size and composition. Figures 13 and 17 illustrated the fact that larger particles polarize to a greater degree. Adams and Filice (1967) showed that larger particles are systematically darker than smaller particles. It is therefore reasonable to assume that the differences in the optical properties between the maria and terrae could be caused by the average particle sizes on the maria being greater than that on the terrae. This hypothesis is now examined in terms of the influence of the mean internal optical path length (IOPL) of the particles on their spectral reflectivity and polarization.

Adams and Filice (1967) determined, for various sizes of pulverized rocks, the ratio of the reflectivity at  $.70 \mu$  to that at  $.40 \mu$ , i.e.,  $R/B$ , and compared it with the reflectivity at  $.50 \mu$ , i.e.,  $V$ . They studied acidic rocks (e.g., rhyolite), rock glasses (obsidian), and basic rocks (basalts). Their results are replotted in Fig. 32. Only basalt powders, they found, showed the trend of increasing reflectivity in the red (increasing  $R/B$ ) with decreasing size for the sizes suspected on the lunar surface ( $<200 \mu\text{m}$ ). The results of reflectivity data collected by Pellicori and Mitchell (1969) on the same lunar

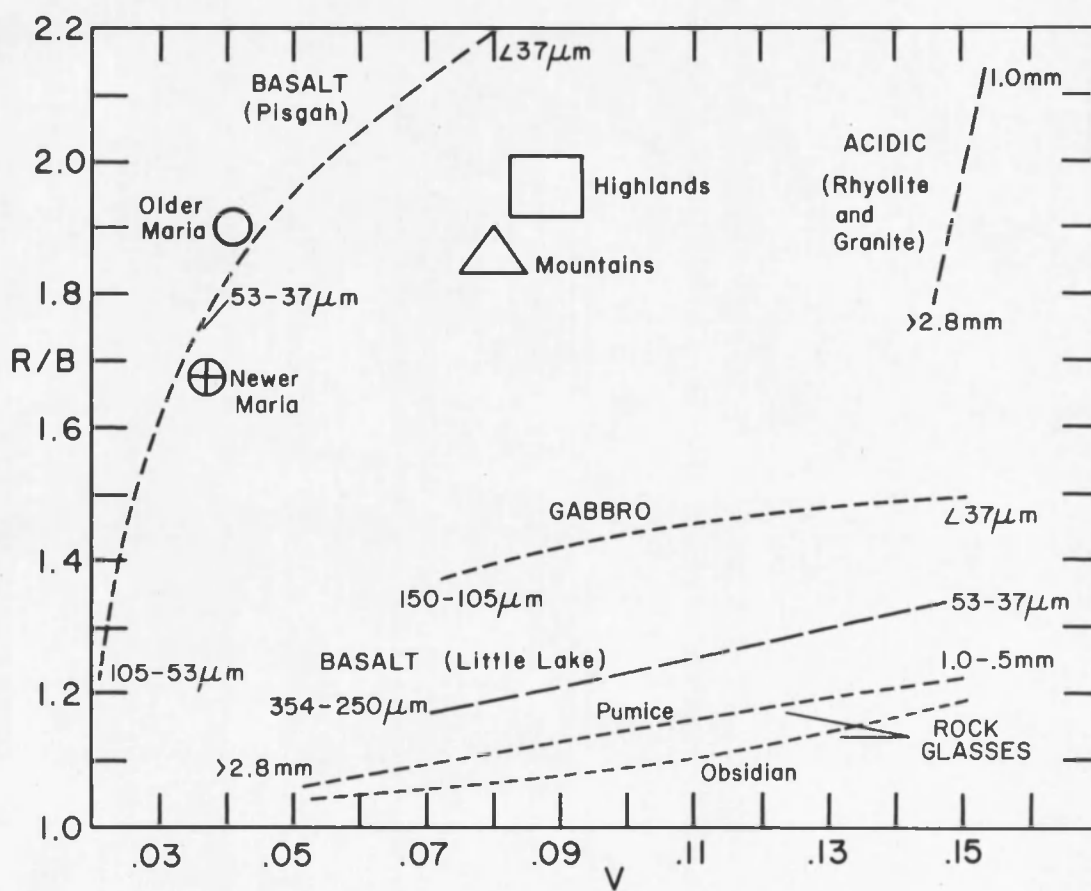


Fig. 32. Reflectivity data of Adams and Filice (1967) replotted.

areas as were observed for polarimetry (Sec. V) are presented, according to topographical type, in Fig. 32. Comparison with the Adams and Filice data supports their conclusion that the lunar materials are basalt, similar to the Pisgah sample, rather than acidic or glassy. Furthermore, particle sizes clustering around 53 to 37  $\mu\text{m}$  are suggested for the maria. The sizes on the terrae are more uncertain, but are perhaps nearer 35  $\mu\text{m}$ . The Pisgah sample, having 3.6% concentration of elements with mass number  $47 < A < 65$ , is darker than the Little Lake basalt (3.1% concentration); both are basic. The Gabbro (San Marcos) has a concentration of 3.3% and is ultrabasic. It has an albedo intermediate between the basic basalts (Franzgrote, Patterson, Turkevich, 1968)

Since the smaller particles are redder, Adams and Filice concluded that the terrae are covered with smaller average particle sizes than the maria. Their explanation for the increase in R/B with decrease in size is as follows.

Consider the Beer-Lambert absorption law

$$I = I_0 \exp (-kd)$$

where  $\underline{k}$  = absorption coefficient,  $\underline{d}$  = physical path length. Then,

$$\frac{R}{B} = \frac{I_R}{I_B} = \exp \{-d (k_R - k_B)\}$$

where  $I_B$  and  $I_R$  are the intensities transmitted with  $(k_R - k_B)$  held constant. As  $\underline{d}$  is increased, R/B decreases; or the light returned is reddened as the particle size is decreased. Smaller particles are more translucent, therefore, light can pass through many such particles

and suffer large selective absorption (be reddened more and more) before reaching the receiver. Therefore, the (redder) terrae have a pre-dominance of smaller particles than the maria (bluer) do.

If, instead, the quantity  $(k_R - k_B)$  is increased while  $d$  is held constant, reddening would again occur. However,  $k_B$  is always greater than  $k_R$  in the optical region, therefore,  $R/B$  would, in reality, decrease. In other words, for highly absorbing particles the light returned is bluer for constant particle size than for the case of translucent particles. Thus the maria are bluer because they have larger particles than the terrae.

The product of absorption coefficient and (internal) physical path length is defined as the internal optical path length (IOPL). Following a line of reasoning similar to that of Adams and Filice for explaining the lunar color differences outlined above, I propose an explanation of the lunar polarization differences as follows.

Section VI shows that the polarization produced by translucent powders is always small compared to that produced by opaque powders (Fig. 26). The depolarizing ability (Fig. 30) is greater for the translucent powders. Smaller particles produce lower polarization values because they have smaller mean IOPL than larger particles, i.e., more of the internally randomly scattered light can escape to dilute the resultant polarization. On the other hand, the mean IOPL for large particles is greater, thus the returned light comes predominantly from the exterior surfaces, giving greater polarization. Thus, the fact that the maria polarize light more strongly than the



terrae is explainable in terms of assuming that the maria have a predominance of particles having greater IOPL than the terrae. Notice that either a greater absorption coefficient or greater particle size can make the IOPL large. Thus far we have no conclusive indication through polarimetry or photometry alone as to which is determining the difference between the lunar topographies.

The results of the Surveyor chemical analyses (Franzgrote, et al., 1968), as outlined in Sec. II provide evidence that the maria have approximately twice the concentration of elements with atomic mass number 47-65 that the terrae have. It is these transition metals that give terrestrial rocks their dark colors. Illustration of the influence of absorption coefficient on polarization is provided by Fig. 26: where sulfur is translucent (yellow light) the polarization is small. At wavelengths less than 3800 Å the polarization increases, until, when the light is totally absorbed ( $\lambda < 3700$  Å), the polarization value levels off to a maximum equal to that of (opaque) carbon. I predict, on the basis of the observations in Sec. VI that the lunar curve of Fig. 7 will level off at some maximum polarization at a wavelength at which the lunar particles are totally opaque, and remain constant for all shorter wavelengths. The wavelength at which the curve will level off appears to occur just below 3100 Å.

There is stratigraphic evidence (Strom and Fielder, 1968) that the terrae sample - north slope of Tycho - is actually a late lava flow, and therefore the chemical analysis may not necessarily be representative of typical terra. In spite of this doubt, such a compositional

difference could explain the brightness difference between topographies without appealing to particle size differences. Hartmann concluded (1968), on the basis of crater densities in the bright impact craters Tycho, Aristarchus, and Copernicus, that they are 1/20 to 1/2 the age of the maria (i. e.,  $0.2$  to  $2 \times 10^9$  yrs.). The presumed solar-wind darkening rate and the mixing rate by meteoritic influx should have darkened the upper microns of the bright ray systems in only  $10^5$  years. This suggests that these mechanisms, which would tend to produce uniform blending in the photometry, are of minor importance. Presumably the bright rays are sprays  $< 10$  m thick of finely pulverized particles and must be mixed to at least centimeter depths before they are erased.

Exact measurements of the polarizing properties of samples with known composition differences which reproduce the Surveyor analyses would have to be made to determine if the associated differences in absorption coefficient are sufficient to account for the observed polarization differences without necessitating size differences.

#### Hypothetical Explanation for the Dependence of Polarization on Phase Angle

The large influence of phase angle on the optical properties of rough surfaces was shown for the Moon in Sec. IV and Sec. V, and for laboratory surfaces in Sec. VI although these surfaces were studied only over a small range of angles. The change in shadowing of the particles and spaces of these complex surfaces caused by changing phase angle is responsible for the photometric function. Figures 9 and 10 show powdered surfaces of a pulverized basalt prepared as described

in Sec. VI (i.e., not a "fairy castle" structure) at two phase angles:  $0^\circ$  and  $55^\circ$ . Notice that at  $0^\circ$  there are no shadows, therefore the powder is bright because the light that enters the cavities can escape at emergence angle  $0^\circ$ . At  $\alpha = 90^\circ$  ( $i = e = 45^\circ$ ) very little of the light incident on the microstructure can escape, and the surface is darker. Hapke (1966) provided an analytic expression consisting of the Lambert and the Lommel-Seeliger scattering laws plus some geometry terms applied to fairy castle structures to reproduce the lunar photometric function.

On the basis of laboratory investigations (Sec. VI) concerning the influences of internal and external scattering on the polarizing properties, I suggest a physical model of the polarizing mechanism of complex surfaces. Figure 33 is a sketch of a vertical cross section through the microstructure built from micro-meter size particles. At  $90^\circ$  phase angle ( $i = 45^\circ$  and  $e = 45^\circ$ ) it is highly probable that a light ray must undergo several reflections in order to escape from the structure to the direction of the receiver. Because of the random orientation of the scattering surfaces, incident rays will be scattered in all directions and only a small fraction will be seen by the observer. Generally, at least two reflections are required to send a ray to the receiver. These external reflections produce high polarization (near 50%) as we have seen. Furthermore, it is probable that only facets orientated statistically normal to the plane of scattering will contribute to the light seen by the receiver. A greater percentage of the rays which enter a particle must undergo at least two internal

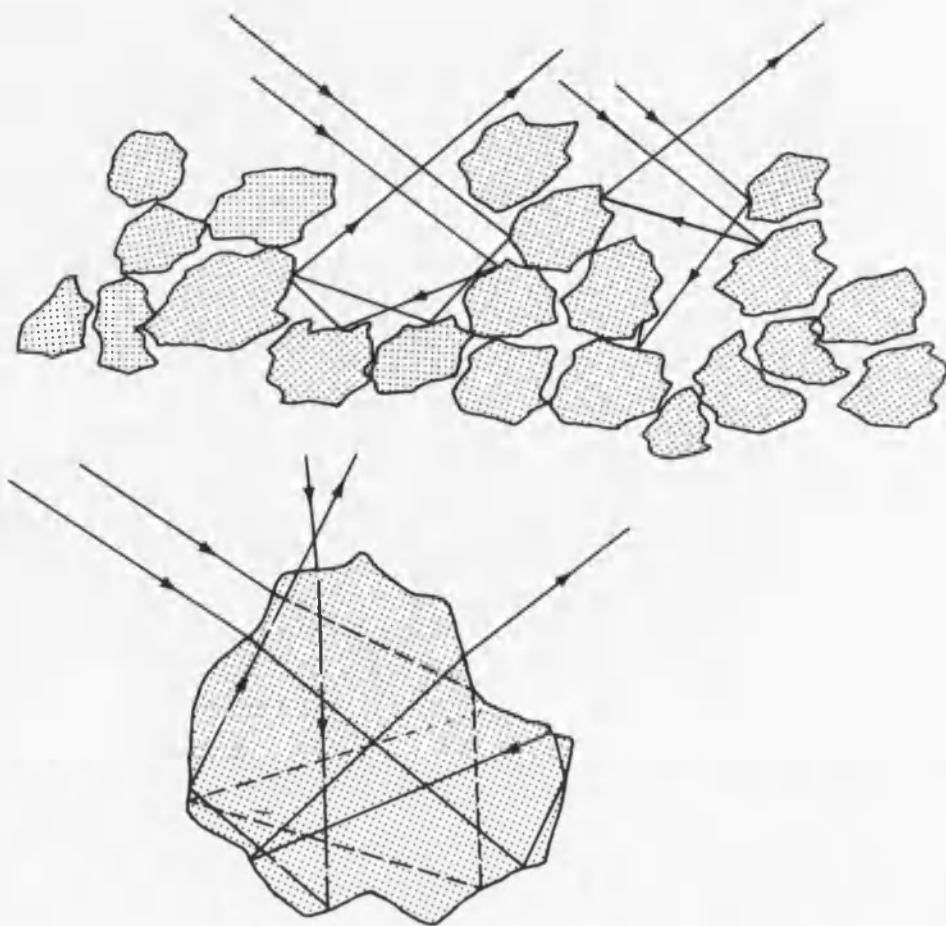


Fig. 33. Vertical cross section through microstructure of surface built from micro-meter size particles.

reflections in order to escape at  $90^\circ$  ( $\epsilon=45^\circ$ ), thus the path length of a ray is large. Since, on the average, the angle of incidence to each facet from within the particle will be large for  $\alpha = 90^\circ$ , total internal reflection is likely to occur. In spite of the fact that these reflections are efficient, the IOPL is large because of absorption within the particle. Consequently, light rays are less likely to return from the interior of a particle seen at  $90^\circ$  phase angle. Recall that this internal component has low polarization and dilutes the measured polarization if allowed to contribute to the total light.

For rays incident near  $i = 0^\circ$  a ray will, on the average be incident on a facet of a particle at a small angle to its normal (since the particles have convex rather than concave shapes) (Fig. 33). Similarly, the internal angles of incidence will, on the average, be small and, therefore, the ray has more chance to escape with only moderate attenuation because its physical path length will not be large. Since the external angles of incidence and emergence are small, the polarization by external scattering will be small. Also, there will be a greater probability that the electric vector of the scattered radiation will be randomly orientated because the reflecting facets seen by the observer are statistically more randomly orientated for  $i$  near  $0^\circ$  than for large phase angles. The changing ratio of externally scattered (and thus highly polarized) light to internally scattered (low polarization) light with phase angle produces, I suggest, the phase-angle dependence of the polarization from pulverized surfaces. Apparently, the external and internal contributions are equal and opposite and thus

cancel at  $\alpha = 23^\circ$  for the Moon (Fig. 4). This suggestion conflicts with the conclusion of Dollfus (1962) who said that because the particles are opaque, negative polarization must be caused by multiple external scattering.

Reference to Fig. 30, showing the depolarizing efficiencies of opaque and translucent materials, reveals that the truly opaque carbon particles do not, as a surface, polarize light to a greater degree than 60% at  $\alpha = 90^\circ$ . Multiple external scattering among neighboring particles must be responsible for this imperfection. This is a reasonable assumption in view of the random statistical nature of the orientation of the microfacets of the particles.

Check of the Hypothesis With Respect to the Phase Angle  
Dependence of the Lunar Colors

Gehrels, et al. (1964) discovered that as the lunar phase angle increases the lunar surface reddens according to

$$B - V = 0.838 + .0017 |\alpha| ,$$

where  $B$  and  $V$  are the blue and visual magnitudes. This effect is explainable in terms of the change in optical path length with phase angle following the argument of Adams and Filice. We have discussed above how  $(k_R - k_B)$  decreases with greater physical path length (blue light is absorbed more highly than red), and thus  $R/B$  increases.

A further check on the influence of external scattering on polarization can be made by comparisons of negative polarization values at two extreme wavelengths. In Table VI are listed some values of negative polarization at two phase angles and at wavelengths  $.36 \mu$  (U)

TABLE VI. Percentage Polarization of Regions at Small Phase Angles.<sup>a</sup>

Region	Filter <sup>b</sup>	Phase angle	Phase angle
		-12° to -15°	+16°
M. Humorum	U	0.93 ± .06%	0.48%
	I	1.41	1.24
M. Imbrium	U	0.96	0.47
	I	1.46	1.19
M. Crisium	U	0.52	0.73
	I	1.23	1.39
Plato (floor)	U	0.78	0.69
	I	1.31	1.29
Near Copernicus	U	0.86	0.62
	I	1.16	0.76
Copernicus	U	0.56	0.56
	I	1.31	0.59
Clavius	U	0.78	0.89
	I	0.69	0.79
Maria <u>averaged</u>	U	0.80	0.59
	I	1.35	1.28
Highlands <u>averaged</u>	U	0.73	0.69
	I	1.05	0.71

<sup>a</sup>From Gehrels, et al. (1964).<sup>b</sup>U is .36  $\mu$ ; I is .99  $\mu$  effective wavelengths.

and  $.99 \mu$  (I) determined by Gehrels, et al. (1964). Notice that the degree of polarization is greater for the longer wavelengths, in opposition to the observations for positive polarization. I propose that this is explainable because there is less shadowing at small phase angles than near  $\alpha = 90^\circ$ , therefore a lower order number of multiple surface reflections will contribute light to the receiver. Since the effective refractive index for blue light is greater than for red, the reflections will be more efficient for the short wavelengths. Therefore, relatively more blue light will be scattered at the statistically small angles of incidence. Thus the greater chance that the short wavelengths are randomly scattered and thus depolarized more than the longer wavelengths.



## SECTION VIII

### CONCLUSIONS

#### Summary

In this study the polarization characteristics of the integrated disk of the Moon, of specific lunar topographies, and in the laboratory of volcanic basalts and pure chemicals were presented in Secs. III, IV and VI. The design of an automatic polarimeter for obtaining more definitive information on the wavelength and phase angle dependences of the polarization of integrated Moonlight was described in Sec. III.

For the intercomparison of the specific lunar topographies, the phase angle range was restricted to the region of maximum polarization, and the wavelength dependence over the range 3200 to 5500 Å was illustrated in Figs. 7 and 8.

Observation of the optimal values of the variable parameters (wavelength and phase angle) revealed small differences between the wavelength dependences of the polarization of the lunar maria (older and newer), the mountains, and the highlands (cratered uplands). Specific data are presented on these topographies to assist future research and interpretations concerning the lunar surface.

Interpretation of these differences required a specific laboratory study on pulverized materials where, as with the lunar observations, some of the independent variables were fixed at their most

influential values. Low density surfaces made from pulverized basaltic lavas and chemicals (controlled composition) were studied to define the influences of particle size, composition, state of surface compaction, and wavelength on the polarization at 90° phase angle. The phase angle of maximum polarization was determined also as a function of the preceding dependent variables (see Sec. VI).

It was found that materials having large internal optical path lengths will scatter light with a large polarization because all of the returned light has been scattered from external surfaces. Translucent materials or smaller particles produce lower polarization. Therefore, the roles of external and internal scattering were defined in terms of particle size and composition (i. e., the combined effect which is responsible for the internal optical path length). From the observation that even the darkest lava, when reduced to a size distribution expected for the lunar particles ( $<74\mu\text{m}$ ), was translucent and not completely absorbing, and from comparisons of the wavelength dependence of polarization with that for the Moon, it was concluded that the lunar particles must be translucent and not opaque. Lava particles are translucent, as was confirmed by photomicrography and by spectral transmission traces to short wavelengths. The wavelength dependence of the polarization of the Moon and of similar surfaces such as Mercury, Mars, and the asteroids is explained in terms of the increasing internal optical path lengths of the particles as the wavelength is decreased, thereby increasing the ratio of external scattering (highly polarizing) to internal scattering (lower polarization) as the wavelength is decreased.

The use of the value of the phase angle for maximum polarization as a tool for unambiguous identification of particle composition was shown to be invalid because this parameter was found to be a function of particle size and state of surface compaction. The angle is, however, sensitive to the detection of a constituent having a reasonably different maximum angle from other constituents, even though the materials are not separable on the basis of the polarization-vs-wavelength (at fixed phase angle) curve of the mixture.

Brewster's law, and therefore, inferentially, Fresnel's reflection laws, were shown empirically to be inapplicable to surfaces of pulverized materials and thus to the lunar surface because no systematic correlation was found between refractive index and phase angle of polarization maximum.

The final pages extend the finding of the influences of particle internal optical path length on the polarizing properties, and hypothetically explain the dependence of these properties on phase angle and wavelength for the lunar characteristics.

#### Recommendations for Future Research

The polarizing properties of samples such as studied here should be determined over a greater range of wavelengths, preferably approaching  $0^\circ$ . This study was restricted to volcanic lavas, but, as pointed out in the text, the rate of solidification probably affects the optical properties and thus volcanic ashes (fast rate of cooling) should be included in future studies.

Although little will be learned about polarization mechanisms by studies at longer wavelengths where materials have little overall absorption, the polarization vs. wavelength curves for silicate rocks, for example, should be extended to the region 1 to 20  $\mu$  because many of them have absorption bands in this region. Since the polarizing properties are sensitive to sudden increases in internal optical path length, the detection of absorption bands in lunar materials, for example, could be assisted by high spectral resolution polarimetry.

More work is needed toward understanding the causes of negative polarization. The role of diffraction on the lunar surface, especially at large phase angles (forward scattering), needs to be defined.

More measurements on pure examples of lunar topography should be made with extension to a greater phase angle range. Interesting lunar regions such as more recent impact craters and their rays, and areas of suspected recent volcanic activity, should be studied.

Polarimetry to wavelengths shorter than 3000 Å should be undertaken on laboratory samples. According to my prediction, at those wavelengths at which none of the internally scattered light can escape from a particle the polarization should level off to a stationary value. Extension of the wavelength dependence measurements to shorter wavelengths in order to verify this thesis can be achieved with a high altitude balloon flight of the automatic polarimeter described in Sec. III.

A direct test of the translucency hypothesis will be available when actual samples of lunar grains are collected. This, according to the recent time schedule, will occur within eight months of this writing.

# LIST OF REFERENCES

- Adams, J. B., and Filice, A. L. 1967, J. Geophys. Res. 72, 5705.
- Arago, F. 1811, Oeuvres 10, 564.
- Barabashev, N. P. 1926, A. N. 229, 7.
- Barabashev, N. P., and Chekirda, A. T. 1956, Astr. Zh. (Sov. Astron.-AJ) 33, 549. (Translation RSIC-403, Redstone Scientific Information Center, 1965).
- Billings, B. H. 1951, J. O. S. A. 41, 966.
- Born, M., and Wolf, E. 1965, Principles of Optics, (Oxford: Pergamon Press).
- Brewster, D. 1861, Trans. Roy. Soc. Edinburgh XXIII, 205.
- Clarke, D. 1964, Astron. Contrib. Univ. Manchester Series III, No. 107.
- Coffeen, D. L. 1965, Astron. J. 70, 403.
- Coyne, G. V. 1965, Astron. J. 70, 115.
- Coyne, G. V., and Pellicori, S. F. 1969, in preparation for Astron. J.
- Cruikshank, D. P. 1968, Infrared Colorimetry of the Moon, Ph. D. thesis, University of Arizona.
- Dollfus, A. 1955, Tech. Transl. F-188, NASA, Washington, D. C., 1964.
- Dollfus, A. 1962, Physics and Astronomy of the Moon, Ed. by Z. Kopal, (New York and London: Academic Press, Inc.).
- Egan, W. G. 1967, J. Geophys. Res. 72, 3233.
- Egan, W. G., and Smith, L. L. 1965, Grumman Research Dept. Memorandum RM-304.
- Egan, W. G., Smith, L. L., and McCoyd, G. C. 1966, Grumman Research Dept. Report RE-250.

- Franzgrote, E. J., Patterson, J. H., and Turkevich, A. L. 1968, in Surveyor VII Mission Report, Pt. II, J. P. L. Tech. Report 32-1264, 241-265.
- Galileo, G. 1632, Dialogue Concerning the Two Chief World Systems-Ptolemaic and Copernican, Transl. by S. Drake, 1967, (Berkeley and Los Angeles: University of California Press).
- Gault, D., Collins, R., Gold, T., Green, J., Kuiper, G. P., Masursky, H., O'Keefe, J., Phinney, R., and Shoemaker, E. M. 1967, Surveyor III Mission Report, J. P. L. Tech. Report 32-1177, 200-203.
- Gehrels, T. 1959, Astron. J. 64, 332.
- Gehrels, T., Coffeen, T., and Owings, D. 1964, Astron. J. 69, 826.
- Gehrels, T., and Teska, T. M. 1960, Pub. Astron. Soc. Pac. 72, 115.
- Greer, R. T., and Hapke, B. W. 1967, J. Geophys. Res. 72, 3131.
- Hapke, B. W. 1962, Second Preliminary Report on Experiments Relating to the Lunar Surface, Center for Radiophysics and Space Research, Report No. 127.
- Hapke, B. W. 1966, Astron. J. 71, 333.
- Hapke, B. W. 1968, Planet. Space Sci. 16, 101.
- Hapke, B. W., and Van Horn, H. 1963, J. Geophys. Res. 68, 4545.
- Hartmann, W. K. 1968, Comm. Lunar and Plan. Lab. 7, 145.
- Hovis, W. A., Jr., and Callahan, W. A. 1966, J. O. S. A. 56, 639.
- Ivanov, A. P., and Toporets, A. S. 1956, Soviet Phys.-Tech. Phys. 1, 598 and 605.
- KenKnight, C. E., Rosenberg, D. L., and Wehner, G. K. 1967, J. Geophys. Res. 72, 3105.
- Kohan 1962, The Moon, Ed. by Z. Kopal and Z. K. Mikhailov, (London and New York: Academic Press, Inc.), p. 453.
- Kruger, W. 1903, Sirius 36, 145.
- Landerer, J. J. 1890, Compt. Rend. 109, 360.
- Lipskii, Yu. N., and Pospergelis, M. M. 1967, Sov. Astron.-AJ 11, 2.
- Lyot, B. 1929, Tech. Transl. F-187, NASA, Washington, D. C., 1964.

- McCord, T. B. 1968, Color Differences on the Lunar Surface, Ph. D. thesis, California Institute of Technology.
- Nash, D. B. 1967, J. Geophys. Res. 72, 3089.
- Ohman, Y. 1945, Arkiv. Math, Astron., Fysik 32, 1.
- \_\_\_\_\_ 1955, Stockholm Obs. An. 18, No. 8.
- Parsons, W. 1878, Sci. Proc. Roy. Dublin Soc. 1, 19.
- Peacock, K. 1968, Icarus 9, 16.
- Pellicori, S. F. 1969, Nature 211, 162.
- Pellicori, S. F., and Gray, P. R. 1967, Appl. Opt. 6, 1121.
- Pellicori, S. F., and Mitchell, R. I. 1969, in preparation for Astron. J.
- Pellicori, S. F., Roland, E. H., and Teska, T. M. 1965, Rev. Sci. Instr. 36, 611.
- Provostaye, and Desain 1852, Ann. Chim. Phys. (3) 34, 220, quoted in Umov, N. A. (1905).
- Salet 1922, L'Astronomie, p. 408.
- Secchi 1859, Mon. Not. Roy. Astron. Soc. 19, 290.
- Stair, R., and Johnston, R. 1953, Bur. Std. J. Res. 51, 81.
- Strom, R. G., and Fielder, G. 1968, Nature 217, 611.
- Sytinskaya, N. N. 1956, Astron. Tsirk. 168.
- Teyfel, V. G. 1959, Astron. Tsirk. 205, 7-8.
- Umov, N. A. 1905, Phys. Zeit. 6, 674.
- Van den Bergh, S. 1962, Astron. J. 67, 147.
- Verdet 1860, Optique Physique 2, 488.
- Wehner, G. K., Rosenberg, D. L., and KenKnight, C. E. 1964, Investigation of Sputtering Effects on the Moon's Surface, Fifth Quarterly Status Report, Applied Science Div., Litton Systems, Inc.

Whitaker, E. A. 1965, Ranger VII Experimenter's Analysis and Interpretations, J. P. L. Tech. Report 32-700, 26-29.

Woronkoff, G. P., and Pokrowski, G. J. 1924, Z. Physik 30, 139.

Wright, F. E. 1927a, Natl. Acad. Sci. U. S. 13, 535.

\_\_\_\_\_ 1927b, Carnegie Yr. Bk. No. 26.

\_\_\_\_\_ 1935, Carnegie Yr. Bk. No. 34.

\_\_\_\_\_ 1936, Carnegie Yr. Bk. No. 35.

\_\_\_\_\_ 1937, Carnegie Yr. Bk. No. 36.

\_\_\_\_\_ 1938, Carnegie Yr. Bk. No. 37.